SEDIMENTOLOGY the journal of the International Association of Sedimentologists

Sedimentology (2009) **56,** 1226–1249 doi: 10.1111/j.1365-3091.2008.01030.x

Three-dimensional architecture of submarine slide surfaces and associated soft-sediment deformation in the Lutetian Sobrarbe deltaic complex (Ainsa, Spanish Pyrenees)

PIERRE CALLOT*[1,2,3], FRANCIS ODONNE[1,2,3], ELIE-JEAN DEBROAS[1,2,3], AGNÈS MAILLARD[1,2,3], DAMIEN DHONT†, CHRISTOPHE BASILE‡ and GUILHEM HOAREAU[1,2,3]

[1]*Université de Toulouse; UPS (OMP); LMTG; 14 av. Edouard Belin, F-31400 Toulouse, France*

[2]*CNRS; LMTG; F-31400 Toulouse, France*

[3]*IRD; LMTG; F-31400 Toulouse, France (E-mail: callot@lmtg.obs-mip.fr; odonne@lmtg.obs-mip.fr)*

†MIGP, UMR 5212 CNRS – Total – Université de Pau et des Pays de l'Adour, Bat. IPRA, BP 1155, 64013 Pau Cedex, France

‡Laboratoire de Géodynamique des Chaînes Alpines, CNRS-UMR 5025, Observatoire des Sciences de l'Univers de Grenoble, Université Joseph Fourier, BP 48, 38041 Grenoble Cedex, France

Associate Editor – George Postma

ABSTRACT

Five successive fossil submarine slides have been mapped and described in the Sobrarbe deltaic complex (Ainsa Basin, Spanish Pyrenees). These slides affect and remove up to 15% of the delta front. The head of the scar surfaces is recognized clearly in the field due to the angular unconformity between the infilling sediments and the underlying layers. Most of the slide scarps trend 55°N with 20° to 40° dips indicating north-westward sliding. Downslope, traces of the sliding surfaces parallel stratification. However, these surfaces can be identified by displaced masses, resedimented sandstones and soft-sediment deformation features such as metre-scale half-grabens, normal faults and tension cracks; all the surfaces indicate a sliding displacement toward the north-west. A three-dimensional model built from topographic data with Earth Vision® software shows the architecture of the slide surfaces and provides an estimation of the volume of each sedimentary body within the limit of the studied area. This study also indicates that: (i) the sediments have been cut and carried away before their lithification; (ii) the sedimentation rate infilling a single slump scar is estimated to be about 8 m per 1000 years, i.e. 10 times higher than in the overall area of the Sobrarbe deltaic complex; (iii) each composite scar progressively develops and infills by retrogressive slumps; (iv) the successive slide surfaces stack vertically in a collapse complex structure and migrate downward to follow the sea-level drop between two successive collapse complex structures; (v) the development of the scars in the Sobrarbe delta is described from a seven-stage conceptual model starting with a regressive event; and (vi) the triggering of the Sobrarbe instabilities is controlled by high values of sedimentation rate, relative sea-level falls mainly controlled by tectonic uplift, and likely seismic activity.

Keywords 3D modelling, Ainsa Basin, fossil submarine slides, sedimentary instabilities, seismite, slope instabilities, soft-sediment deformation, tsunamite.

*Present address: Institut EGID, Université Bordeaux 3, allée Daguin, 33607 PESSAC Cédex, France (E-mail: callot.prof@yahoo.fr).

INTRODUCTION

Slope instabilities are responsible for the remobilization and distribution of sediments on continental margins. Displacement can start by the development of a cohesive slide or slump and evolve to a debris flow as the fragmentation increases during the transport process. The end result may be the development of laminar flow that can transform into a turbidity current which deposits sediments on the distal part of submarine fans along low-gradient slopes (Fisher, 1983; Mulder & Cochonat, 1996; Mulder & Alexander, 2001).

In the last few years, progress in oceanography has provided detailed views of present-day submarine landslides on continental margins (Gardner *et al.*, 1999; Canals *et al.*, 2004; Haflidason *et al.*, 2004; Trincardi *et al.*, 2004; Wilson *et al.*, 2004). Thus, side-scan images, multibeam bathymetry, high resolution or three-dimensional (3D) seismic and sub-bottom profiles have revealed the overall morphology, the basal slope and the complete 3D images of present-day slides on continental margins (Huvenne *et al.*, 2002; Frey Martínez *et al.*, 2005, 2006; Moscardelli & Wood, 2008).

Creeping may slowly displace considerable sediment masses over long distances (Mulder & Cochonat, 1996; Reading, 1996). However, in most cases, movement starts with slides or slumps that often change in more mobile sediment gravity flows with downslope acceleration and dilution by progressive water incorporation and cohesion loss (Mulder & Alexander, 2001).

The initiation of these submarine landslides is controlled by the slope failure conditions (Mandl & Crans, 1981), that include internal and external parameters. The most important internal physical parameters are the cohesion, the internal friction coefficient of the sediments and the pore-fluid pressure (Mandl & Crans, 1981; Mello & Pratson, 1999; Mourgues & Cobbold, 2003). These parameters can evolve during diagenesis, resulting in progressive porosity changes (Porebski & Steel, 2003). A sudden increase in pore-fluid pressure may result in a decrease in the sediment shear strength and in a reduction in effective shear stresses (Terzaghi, 1943; Spence & Tucker, 1997).

The main external parameters are tectonic setting, seismicity, slope geometry, sea-level changes and sedimentation rates. Tectonic setting and seismicity may be responsible for sudden stress increase or sediment liquefaction (Field *et al.*, 1982; Greene *et al.*, 1991; Papatheodorou & Ferentinos, 1997; González *et al.*, 2004). The result is a reduction in shear strength of the sediment induced by an increase in pore-fluid pressure triggering slope instabilities (Allen, 1982; Nichols, 1995; Chapron *et al.*, 1999; Piper *et al.*, 1999; Locat & Lee, 2002; Sultan *et al.*, 2004). The dip value of the slope surface may control the shear stresses applied to the sediment (Mandl & Crans, 1981). The differential loading of sediments may also result in a differential compaction that causes fluid or gas expulsion (Vendeville & Gaullier, 2003). Moreover, the instability often develops due to the simultaneous association of some of these parameters (Mienert *et al.*, 2002).

Both present-day submarine landslides and fossil slides provide complementary information to help the understanding of instability processes. The study of present-day submarine landslides provides data on the surface geometry and extension, on the timing of the successive events that have built the sliding and on the volume of displaced sediments. When compared with present-day submarine landslides, fossil slides provide details of the internal structures, deformation and depositional processes (Martinsen, 1989; Lucente & Pini, 2003; Pickering & Corregidor, 2005; Vernhet *et al.*, 2006; Spörli & Rowland, 2007; Callot *et al.*, 2008). Where the outcrops are well-exposed, the complete vertical succession of the different sliding events can be observed and the subsequent study of their temporal and spatial relationships is then possible.

This paper focuses on fossil submarine landslides of the Lutetian Sobrarbe deltaic complex (Spanish Pyrenees) in order to identify the geometry of the slide surfaces that occurred during the sedimentation. The geological setting of the area has been established previously (De Federico, 1981; Dreyer *et al.*, 1999) and is not developed in this work. Field exposure is very good, particularly in the western limb of the Santa Maria de Buil syncline presently crossed by several small valleys that exhibit sections of the slide surfaces and some of the classical associated structures: scars, tilted blocks, syn-sedimentary faults and microfaults, small-scale slump structures.

Each slide surface has been described in order to present the different structures and deformation processes that can be recognized. The spatial organization of the different slide surfaces and their relationships with local sedimentation has been reconstructed from detailed field mapping and a 3D geological model on the base of very

accurate topographic measurements. The 3D geological model permits an estimate of the initial sediment volumes that can be compared with the sediment volumes removed by the fossil slides. A conceptual model describes the development of the scars in the Sobrarbe delta.

GEOLOGICAL SETTING OF THE EOCENE SOBRARBE DELTAIC COMPLEX

In the central part of the Eocene South Pyrenean Foreland Basin, the Sobrarbe deltaic complex represents the last marine filling of the Santa Maria de Buil syncline as a part of the Ainsa Basin. It is a piggyback basin that has developed westward during the in-sequence formation of three growing lateral thrust-ramp anticlines (Figs 1 and 2). The delta formed west of the north–south anticlinal ridge of Mediano, over the gentle growing Arcusa anticline and east of the Boltaña anticline condensation zone during Lutetian to Bartonian times. The submarine uplift of these anticlines forced sediments to enter within the Buil syncline from the south-east and to prograde towards the north/north-west (Fig. 2; Puigdefabregas *et al.*, 1991; Muñoz *et al.*, 1994; Dreyer *et al.*, 1999).

The sedimentary facies of the Sobrarbe deltaic complex has been described by De Federico (1981), Wadsworth (1994) and Dreyer *et al.* (1999). Six facies associations have been recognized (Dreyer *et al.*, 1999). Most are mudstone-dominated and correspond to delta plain, delta front and slope deposits: (i) slope marlstones and turbidite sandstones; (ii) silty and bioturbated sandstones at the distal delta front; (iii) proximal delta front and delta plain deposits; (iv) biogenic deposits on flooding surfaces; (v) collapse zone deposits; and (vi) Nummulite-dominated shallow-marine carbonates.

Four composite sequences compose the northward prograding Sobrarbe deltaic complex (Fig. 3; Dreyer *et al.*, 1999). These sequences are bounded by regressive unconformities and are composed of numerous minor units bounded by maximum flooding surfaces. Based on the associations of the sedimentary facies, these can be divided into lowstand, transgressive and highstand components. The studied sediments belong to the upper part of the Sobrarbe Formation which includes the top of Comaron Composite Sequence (CCS), the Las Gorgas Composite Sequence (LGCS) and the base of the Barranco el Solano Composite Sequence (BSCS) and in which Dreyer *et al.* (1999, fig. 7) provide two

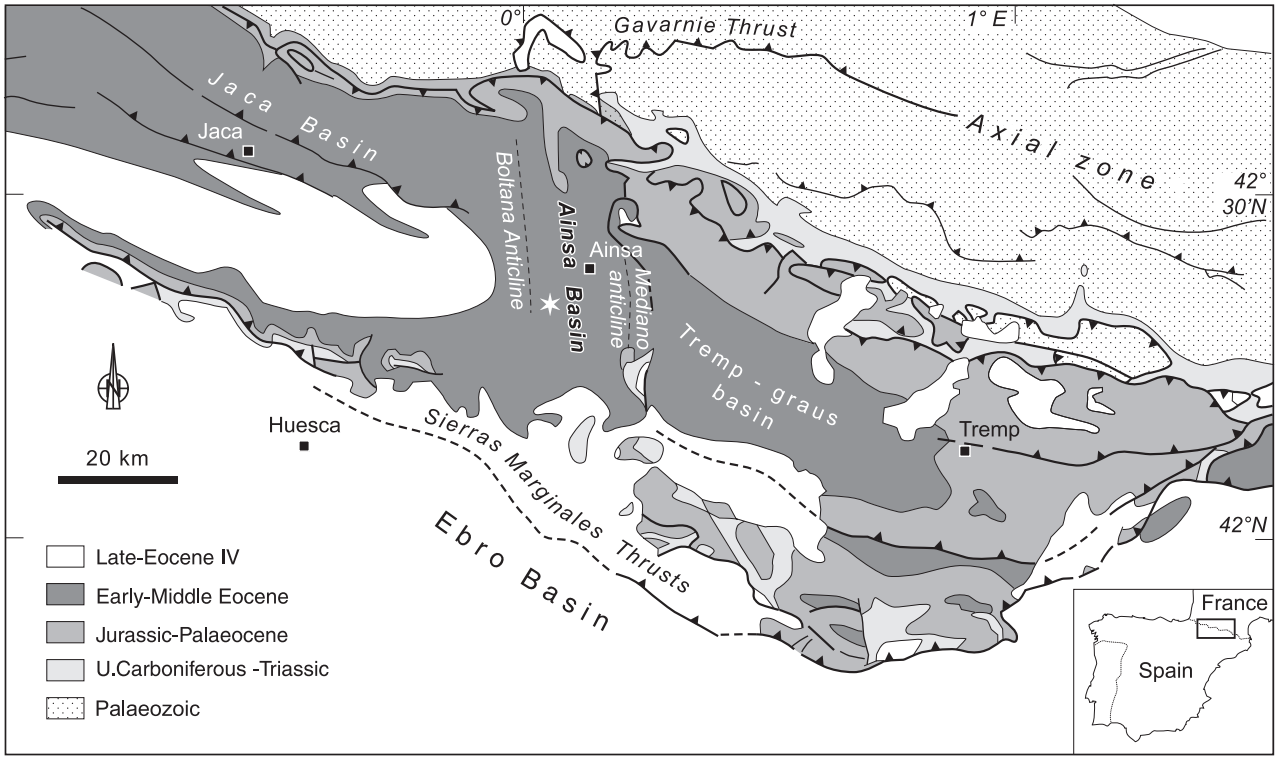

Fig. 1. Simplified geological map of the South Pyrenean Foreland Basin with location of the Ainsa Basin (north of Spain). Redrawn from Dreyer *et al.* (1999). Star indicates the position of the study area.

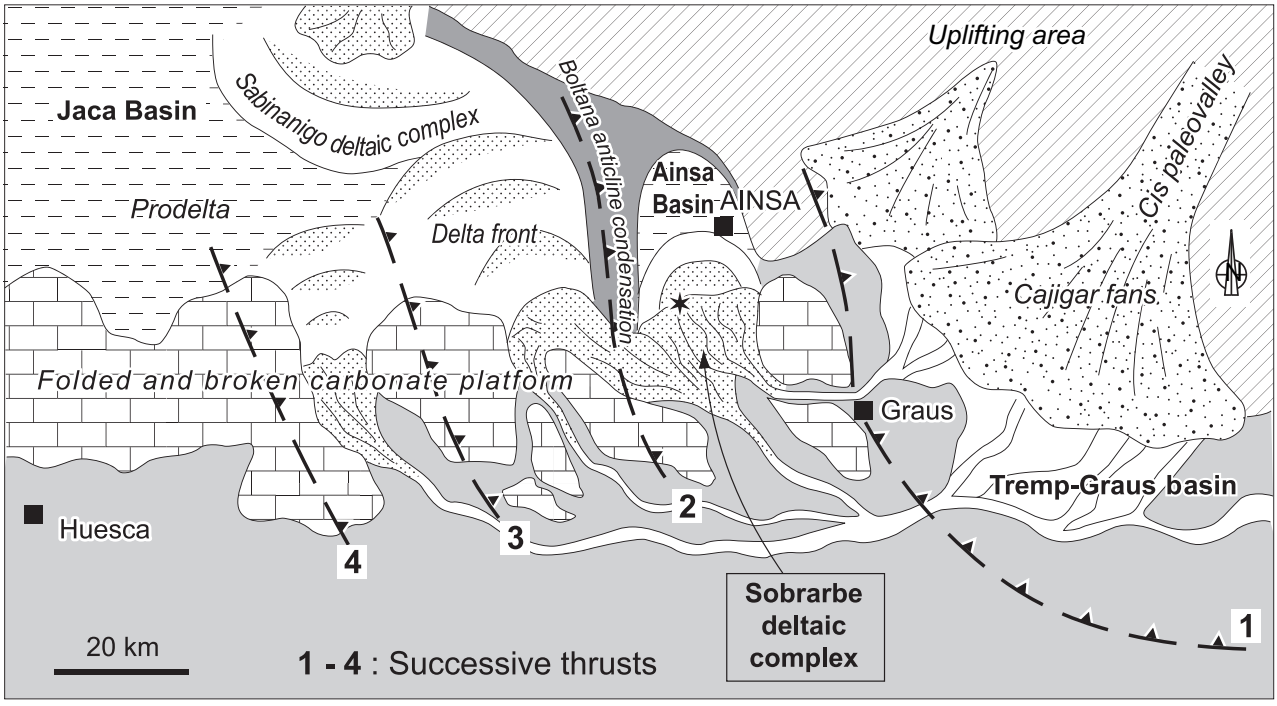

Fig. 2. Palaeogeographic reconstruction of the late Lutetian Sobrarbe deltaic complex in the Ainsa Basin. The successive thrusts form a series of anticlines and synclines that impose the progradation of the sedimentation to the north-west. Redrawn from Dreyer *et al.* (1999). Star corresponds to the study area.

local biostratigraphic timelines: (i) the 'estimated top of the *Nummulites sordensis/N. crassus* biozone' and (ii) the 'estimated top of the *N. herbi/N. aturicus* biozone'. These two timelines correspond to the boundaries of the Shallow Benthic Zone 16 (SBZ 16) correlated with the late Lutetian Chron 19 (around the boundary C19r/C19n) by Serra-Kiel *et al.* (1998). Once updated with the new geological timescale of Gradstein *et al.* (2004) these timelines indicate an age of about 40·8/40·9 Ma for the lower boundary of the SBZ 16 and about 40·4 Ma for the upper one (i.e. Lutetian/Bartonian boundary). Such an age is compatible with data from two recent studies: the mid-Lutetian age of the Ainsa fans and the Lutetian P12 Zone age of the Guaso system deposits (Pickering & Corregidor, 2005) and the Bartonian age of the overlying fluvio-deltaic Escanilla system (Remacha *et al.*, 2003). During this time interval of about 0·4 to 0·5 Ma, about 350 m of sediments have been deposited. The sediment accumulation rate can be estimated as 87·5 to 70 cm per 1000 years, not corrected for compaction. Such values of sedimentation rates are of the same order of magnitude as that observed in modern deltas of the Rhine and Nile (Martinsen, 1989; Loncke *et al.*, 2002).

Numerous gravitational slides have disrupted the layers and have removed 10% to 15% of the delta front strata (Fig. 3). Both the tectonic activity of the growing anticlines and the associated relative sea-level fall are believed to have triggered such sedimentary instabilities (Dreyer *et al.*, 1999; Pickering & Corregidor, 2005). In order to identify the spatial organization of the scar surfaces and the mechanisms responsible for the instabilities, two fossil collapse complexes were focused on: the Barranco el Solano slump and the Fuente Espuña slump scar (Dreyer *et al.*, 1999; Fig. 3).

FIELD IDENTIFICATION OF SLIDE SURFACES

Six main surfaces have been restored and mapped in the collapse complexes of the Las Gorgas and Barranco el Solano Composite Sequences (Fig. 3). The relative positions and extensions of these surfaces are illustrated by the geological map drawn directly on the orthophoto 211-55 of Gobierno de Aragon at a 1:5000 scale (Fig. 4).

Upslope slide area

Most of the slide surfaces are revealed by a correlative upslope angular unconformity (e.g. Figs 5 and 6). The first layers deposited in the scar successively cover the 'sliding blocks' that may

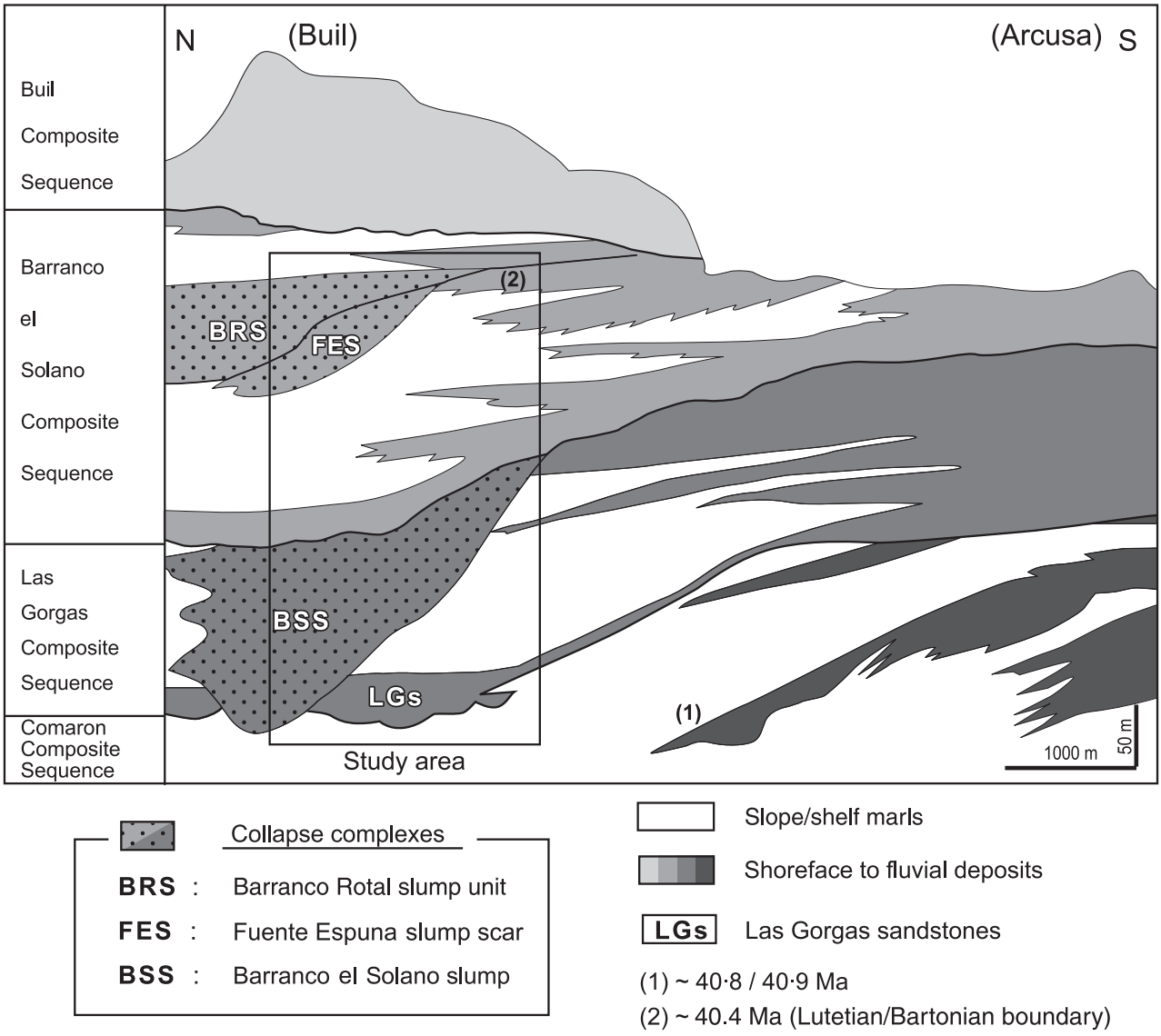

Fig. 3. Correlation diagram of the Sobrarbe deltaic complex in the Ainsa Basin. The slides developed in the Las Gorgas Composite Sequence and in the Barranco el Solano Composite Sequence. (1) and (2): approximate position of the chronological marks; see 'Geological setting' in the text for details. Redrawn from Dreyer *et al.* (1999). The box corresponds to the study area.

Fig. 4. Geological map of the studied area in the western side of the Buil syncline. Six surfaces have been recognized to affect three of the four sedimentary sequences. The S1, S2 and S3 surfaces developed mainly in the Las Gorgas Composite Sequence (LGCS), they were cut and they are filled by the LGCS sediments. The S4 surface developed in the LGCS sediments, the S5 surface developed in the LGCS and the Comaron CS sediments but both are filled by sediments of the Barranco el Solano Composite Sequence (BSCS). The S6 surface developed in the BSCS. In stratigraphic order, the numbers on the legend correspond to: (1) the last deposits of the Comaron Composite Sequence (CCS); (2) the Las Gorgas sandstone body corresponding to the base of the LGCS; (3) the marly distal part of the LGCS; (4) and (5) the deposits – infilling and cover – resting above the S1 and S2 surfaces; (6) the sandy to marly deposits of Biñas d'Ena sequence above the S3 surface with a seismite bed (✺); (7) the first infilling of the Barranco Espuña S4 scar; (7a) Barranco as Peras sandstone body; (7b) Barranco Espuña resedimented and *in situ* deposits; (8) the first infilling of the O Binero S5 scar; (9) the deposits of the BSCS; (9a) last infilling of the S4 and S5 scars; (9b) marlstones and Buil Nummulite banks; (10) the infilling of the Fuente Espuña S6 scar; (10′) the infilling of the Barranco Rotal S6′ scar; (11) the last marine levels of the BSCS and the base of the Buil Composite Sequence (BCS); (12) Quaternary deposits.

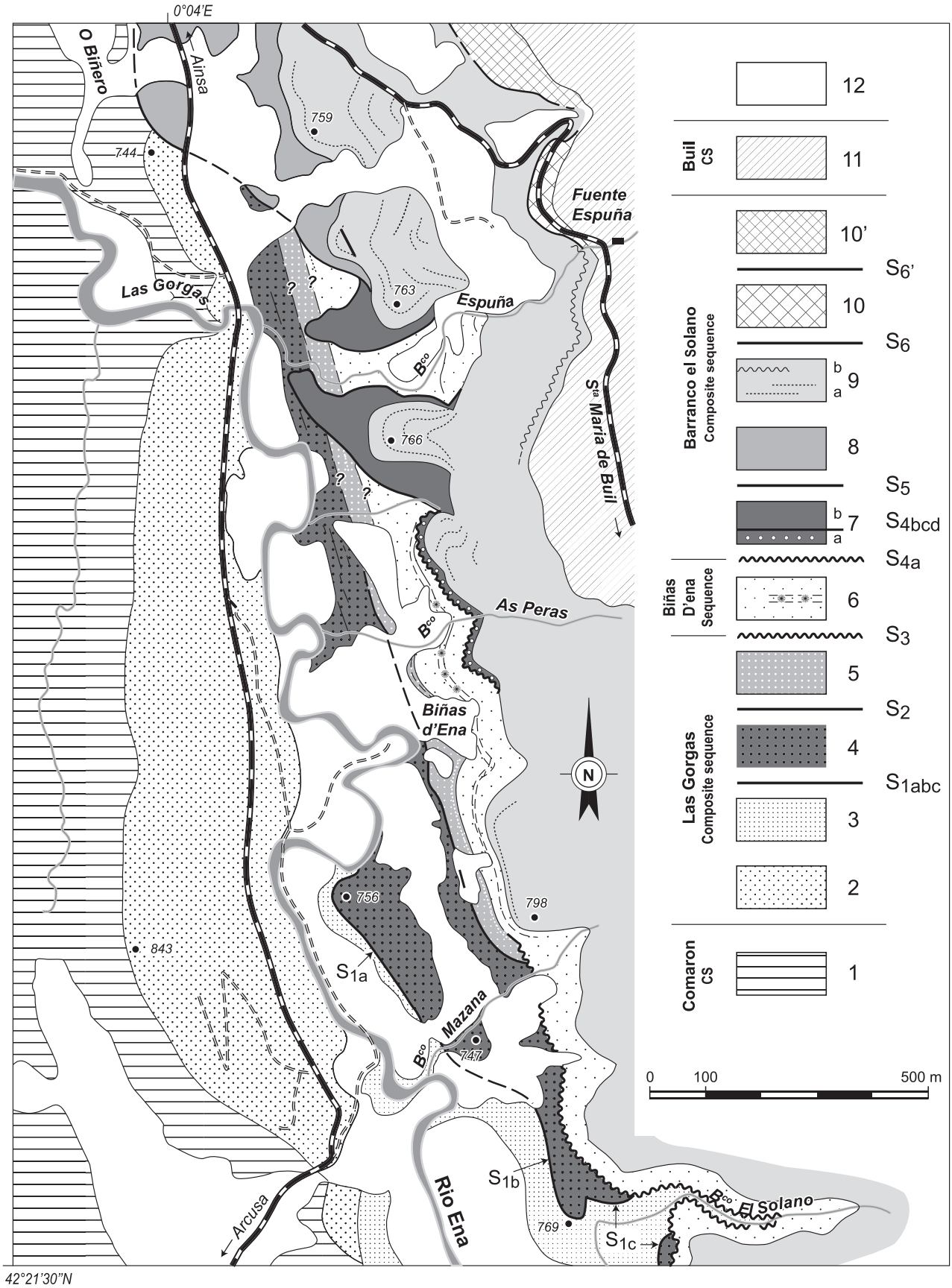

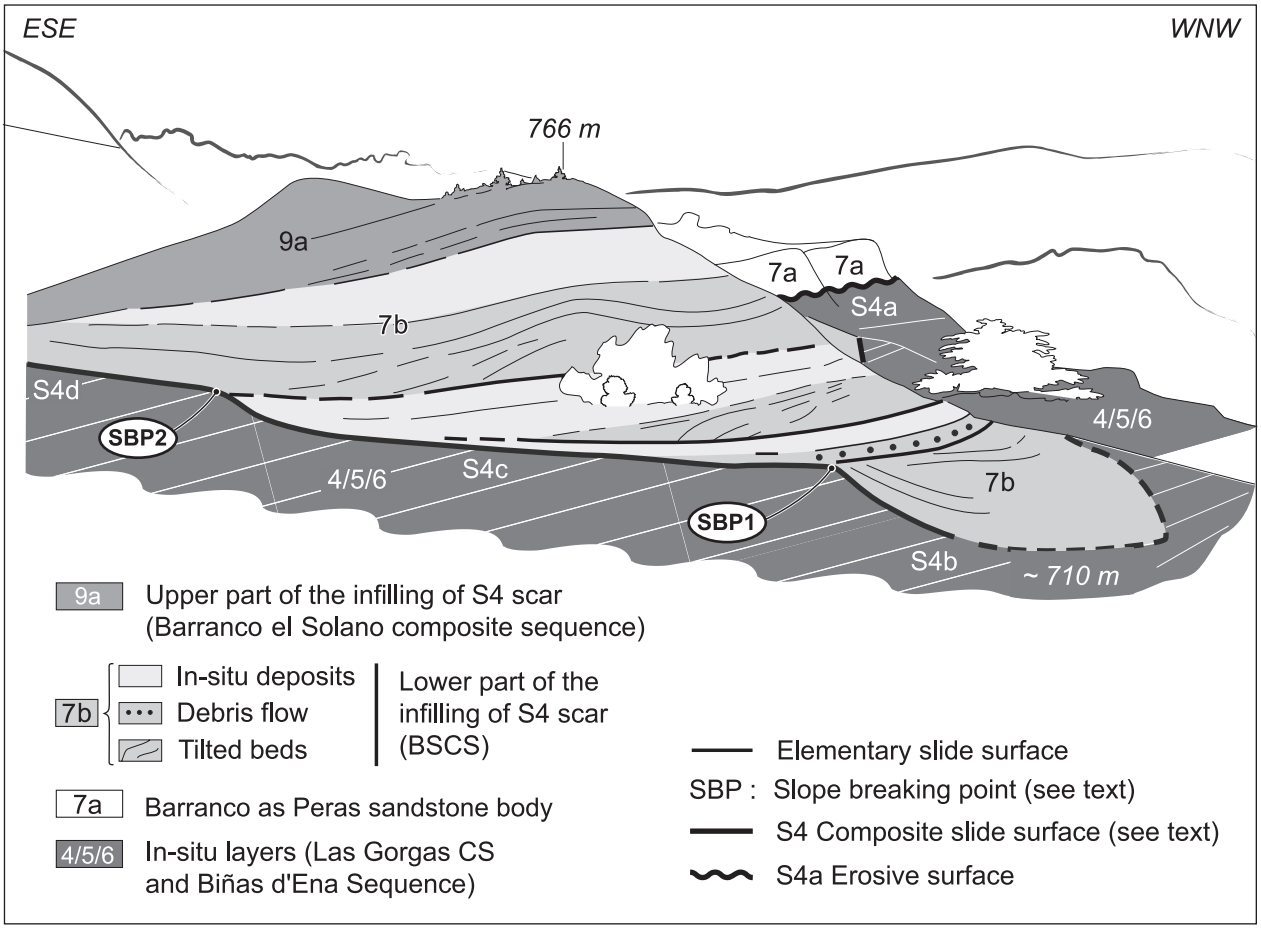

Fig. 5. Line drawing of the composite slide surface (S4) on the left bank of Barranco Espuña. The northern segment of the first-order S4 surface appears to be composed of three segments separated by two slope breaking points. The infilling is subdivided by elementary slide surfaces over which are deposited tilted beds or debris flows draped by apparently *in situ* deposits. Three phases of retrogressive sliding and at least four main phases of infilling can be distinguished. Only the last layers of the infilling, top of 9a, exhibit the same dip values as the *in situ* layers.

rest immediately above the slide surface, onlap the layers truncated by the scar and then drape the remaining slope and its uphill shoulder (Figs 6 and 7). With the progressive infilling, the unconformity reduces upslope and the last deposits are parallel to the *in situ* layers. All these deposits constitute the infill of the slide scar. The overlying deposits constitute the 'cover' (Fig. 7).

Downslope slide area

The angular unconformity between *in situ* and infilling layers progressively reduces downslope where the geometric identification becomes difficult because both *in situ* and infilling layers essentially are parallel. Other indicators of gravitational instability, such as sediment slides and slumps are shown by the presence of displaced and deformed sediments resting above the slide surface (Fig. 7, Area 2) or by deformations in the *in situ* sediments below the detachment surface.

Displaced and deformed sediments resting above the slide surface

Deformed deposits may rest locally above the slide surface; they are composed of cohesive sandstone and/or mudstone layers translated as horizontally bedded rafts (Fig. 6) or as rafts with beds tilted or gently folded during translation (Fig. 5). Rafts are up to 15 m thick and up to 130 m long. Some layers of small to medium-bedded sandstones embedded in mudstones are cut by small normal faults giving a step shape to bedding surfaces (Fig. 8); they look like the closely spaced syn-sedimentary normal faults described by Pickering (1983).

Some thick or very thick beds of debris flow deposits are observed over the slide deposits.

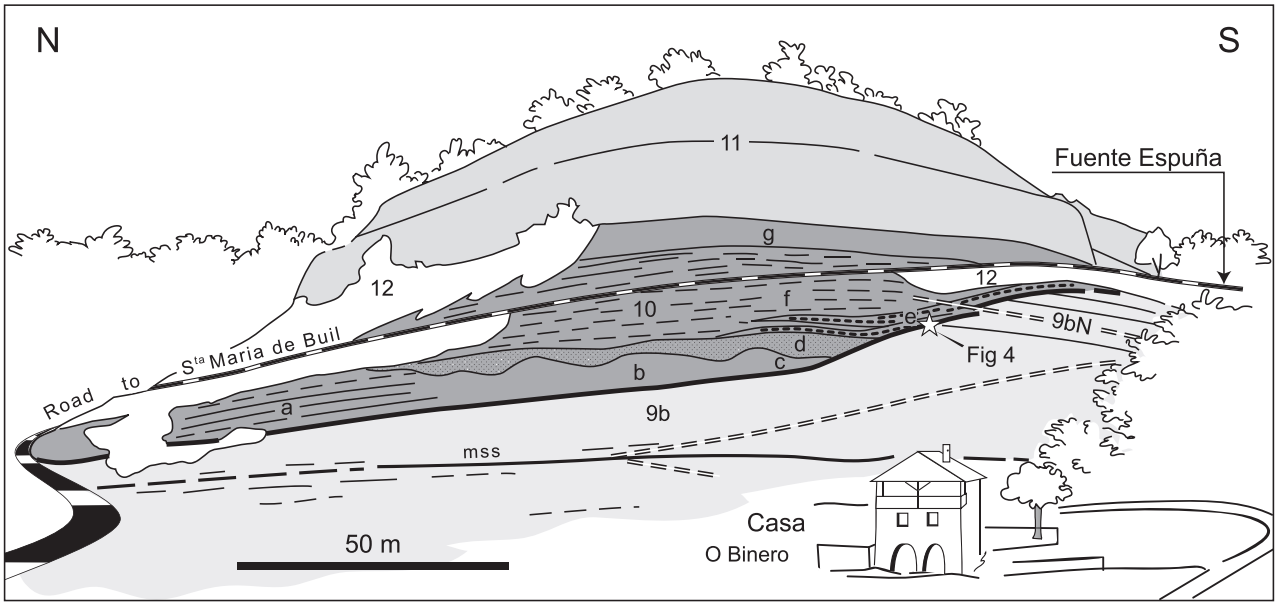

Fig. 6. Line drawing of the Fuente Espuña simple slump scar. The angular unconformity between the S6 surface and *in situ* layers can be observed on both sides of the outcrop (in the south near Fuente Espuña and in the north at the hairpin bend in the road); that indicates a general scarp orientation facing the west. (9b) Named in reference to Fig. 4, *in situ* sandstone and marlstone layers of the Barranco el Solano Composite Sequence (BSCS) with a minor slide surface (mss); (9bN) *in situ* Nummulite banks at the top of BSCS; (10) infilling and cover of the S6 scar: (a) poorly deformed sandy raft; (b) fractured and partly brecciated sandstone bed; (c) complex wedge of slumped layers; (d) wedges of coarse to medium-grained laminated sandstones; (e) Nummulite-rich resedimented marlstones; (f) laminated marls; (g) structureless marlstones with numerous Fe-rich nodules; (11) the last marine levels of the BSCS and the base of the Buil Composite Sequence (BCS); (12) superficial cover.

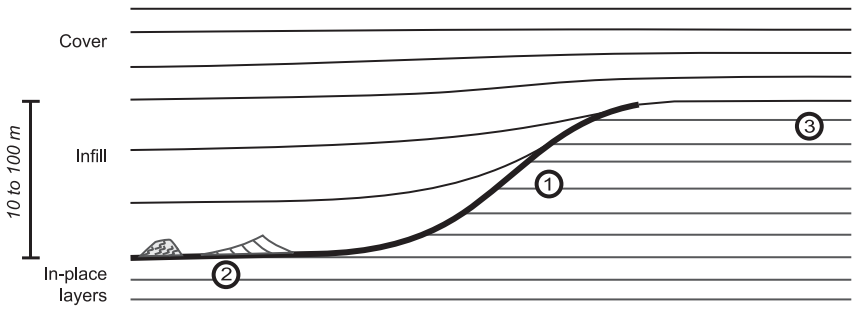

Fig. 7. Schematic line drawing of a simple slide structure. Area (1) corresponds to the head part of the sliding surface where the angular unconformity can reach 45°. Area (2) corresponds to the downslope depression where the angular unconformity progressively reduces and disappears. Slide masses can be observed that rest above the basal slip surface; they are composed of cohesive sandstone and mudstone layers and some of them have been tilted during translation. Area (3) corresponds to the uphill shoulder of the slide where sedimentation is interpreted as having never stopped.

Cohesive debris flow deposits (interpreted as mudflows) are composed of mudstone cobbles and blocks embedded in structureless marlstones. Non-cohesive debris flow deposits (interpreted as grain flows) are composed of structureless sandstone with numerous clay chips. In only a few cases, slump structures with small folds are observed over the studied area and they are limited to thin slump sheets.

Deformation features observed below the slide surface

In some downslope areas, normal faults offset the slide surface up to 2 m (Fig. 9). The *in situ* layers and the main slide surface are tilted. Both the tilted layers and the fault surfaces are covered by horizontal wedges made of structureless and coarse-grained sandstone with clay chips and small plant fragments at the bottom, and of

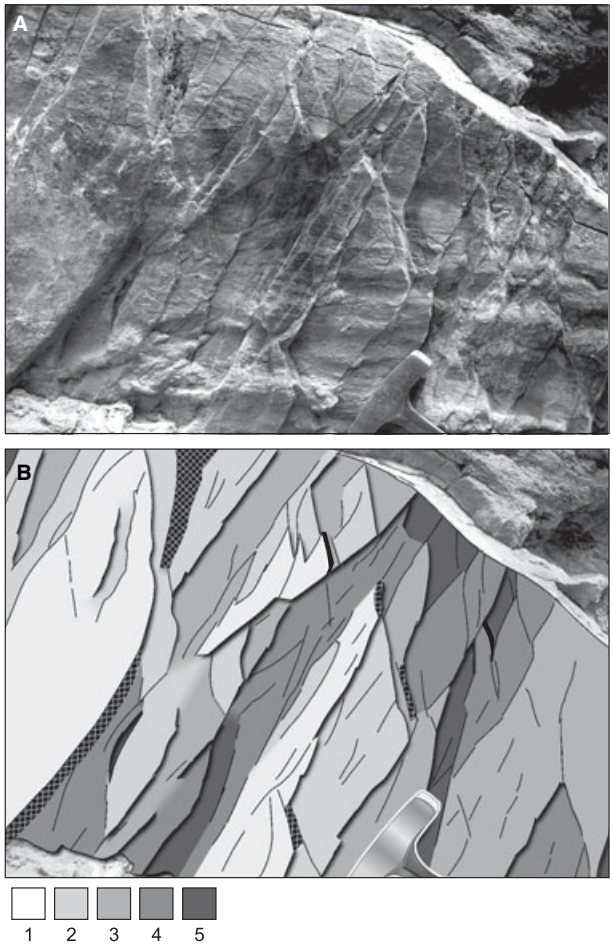

Fig. 8. Soft-sediment faulting of a sandstone bed observed in the infill of the S2 surface. (A) View of a sandstone bed sole that is cut by numerous small normal faults. The visible part of the hammer head for scale is ~10 cm long. (B) Line drawing highlighting the step shape of the same sole. No mineral fibre has been observed on fault planes.

horizontally laminated fine sandstone to siltstone at the top (Fig. 9). These wedges fill small half graben gutters between the fault scarp and the tilted layers. Some flute casts can be observed at the base of the sandstones, striking parallel to the fault and the gutter axis. This kind of erosive basal structure can occur in cohesive but not completely lithified muddy sediments.

The top of the tilted layers is broken by syn-sedimentary vertical dykes. These dykes are parallel to the fault (Fig. 9). Many other dykes have been observed along other sliding surfaces. These dykes all range from 5 to 50 cm width at the top and are up to 2·5 m deep; they are filled by a coarse-grained sandstone similar to the inferred grain flows overlying the sliding surfaces. These dykes seem to be extensive cracks opened by the flexure of the tilted blocks along the outer arc of a rollover structure and can be defined as 'neptunian dykes' (Montenat *et al.*, 1991, 2007; Moretti & Sabato, 2007). The tensile failure of these vertical cracks involved some cohesion of the muddy layers at the time of formation equivalent to mode I rupture (Price, 1966; Engelder, 1987; Price & Cosgrove, 1990).

RESTORATION AND MAPPING OF THE SLIDE SURFACES

Once identified at a point, each of the surfaces has been followed accurately downslope and upslope in the field. In most cases, the distinct surface segments are difficult to link together or to classify in order to restore the geometry of a main surface. The connection of the different segments from facies differences between *in situ* layers and the infilling is not always clear because lateral facies variations are significant along the same main surface. In downslope areas, the Quaternary terraces of the Rio Ena partially cover some sliding surfaces; they were thus mapped from panoramic points of view. In upslope areas, the unconformity, the onlap and the fan shape of the infilling have been used. In such cases, the reconstruction of the slide surface geometry was constrained by the geometry of its banks, as it is not possible to connect directly both sides of a sliding scar (Fig. 10). However, this type of reconstruction must be used with care because: (i) a slide is not necessarily rectilinear, as exemplified by numerous present-day submarine slides (McAdoo *et al.*, 2000; Lastras *et al.*, 2002; De Blasio *et al.*, 2004); and (ii) a scarp head may be confused with the lateral bank of a slide. Consequently, geometric observations must be interpreted in relation to structural observations indicating the displacement direction. Some small isolated outcrops of elementary slide surfaces have not been mapped and integrated into the 3D model because their complete size and correlations are defined poorly. However, detailed observations from these elementary slides can help to understand the triggering mechanisms.

The main slide surfaces of the Sobrarbe delta

Surface S1 can be observed from three segments that are exposed from its upslope part 150 m south of Barranco el Solano to Rio Ena, below point 756 where it disappears under the Quaternary terraces (Figs 4 and 11). This S1 composite

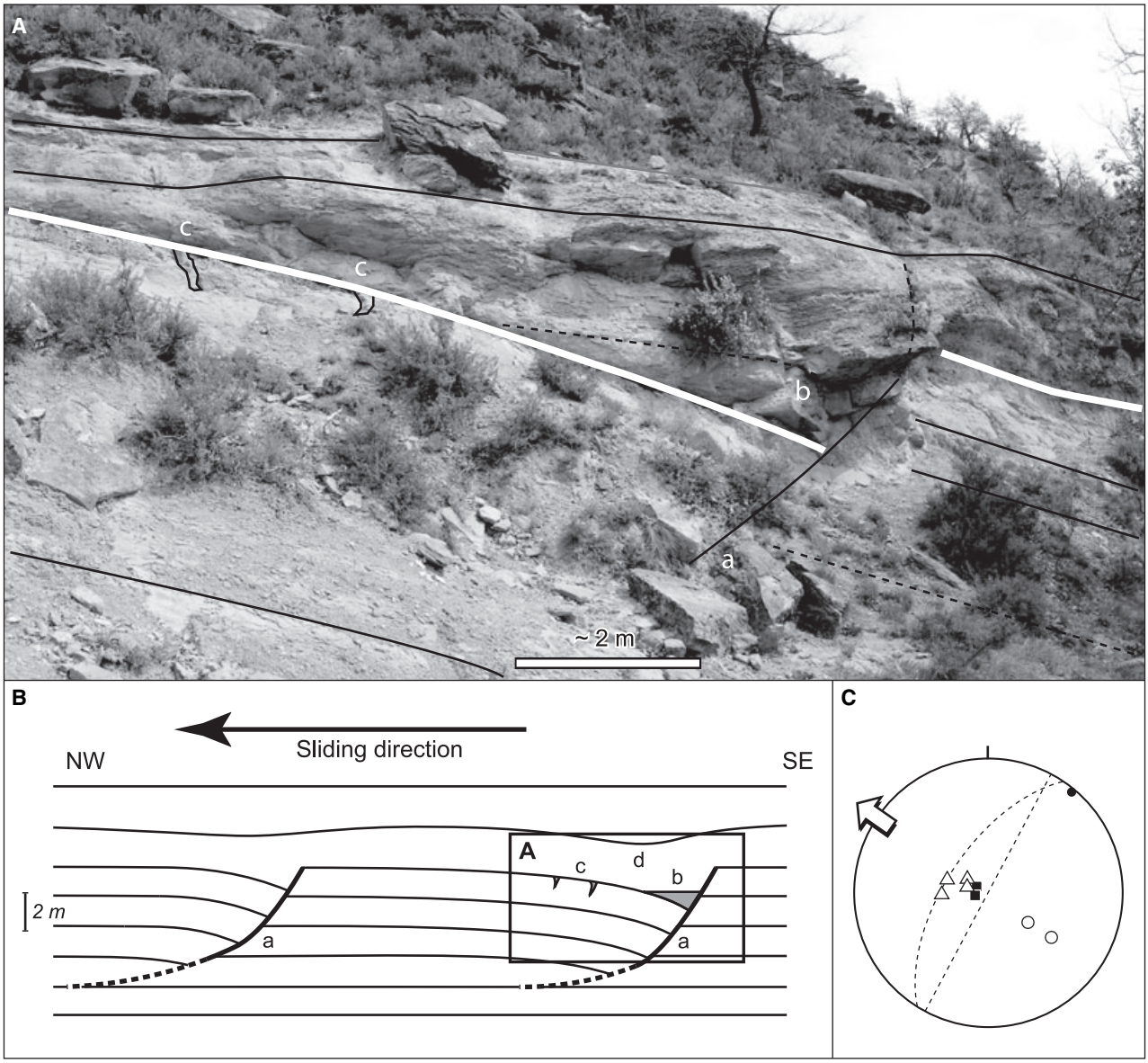

Fig. 9. Soft-sediment normal faults and associated structures affecting the S1 surface (white line) and *in situ* layers surface observed on the right bank of the Rio Ena, below point 756 of Figs 4 and 11. (A) Picture; (B) schematic line drawing of a complete rollover structure composed of: (a) soft listric normal fault orientated 40° N; (b) horizontal wedge of laminated coarse-grained sandstone with clay chips, fine plant fragments and flute casts at the base, which cover both the tilted layers and the fault surfaces over 10 m width, both are orientated 40° N; (c) a few metres away from the fault, on top of the tilted *in situ* layers, thin vertical sandstone 'neptunian dykes' have been formed parallel to the fault; they are filled with the same coarse-grained sandstone as the horizontal wedges, the opening of the vertical dykes involves some cohesion of the muddy layers in which they form; (d) laminated fine sandstones and siltstones. 'b' to 'd' are interpreted as tsunami deposits. (C) Stereographic projection of fault (open circles), footwall layers (black squares), tilted layers (open triangles), vertical dykes (planes) and half graben gutter axis (black dot). The suggested sliding direction points toward the north-west.

surface cuts up to 170 m of the distal marly deposits of the LGCS and is interpreted as overlying the top of the Las Gorgas sandstones in the vicinity of Las Gorgas (Fig. 4).

To the north-west the deepest segment of surface S1 (S1a) exhibits a low angular unconformity between *in situ* and infilling layers and is interpreted as the right bank of the scar. A sliding direction toward the north-west is indicated by the 40° N orientation of normal faults and clastic vertical dykes (Fig. 9). The first part of the infill is composed of a few metres of laminated marls followed by several metres of debris flow deposits with olistoliths and blocks of laminated marls.

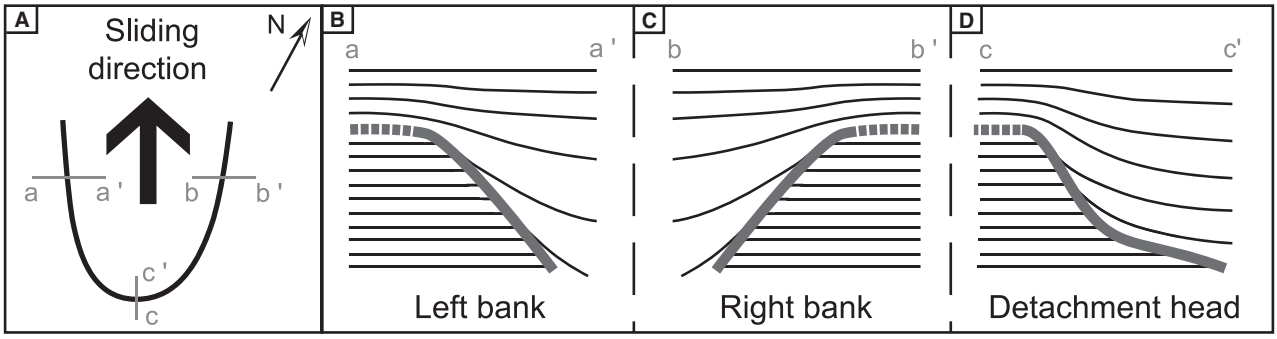

Fig. 10. (A) General shape and orientation of the head scarp discontinuities based on the data shown in Fig. 14. (B), (C) and (D) Polarity of the unconformity according to its position in the slide. (B) and (C) Opposite polarities related to the positions of right banks or left banks of slides have been used to connect the different slide surfaces observed in the Sobrarbe Deltaic Complex. (D) Geometry of the scarp at a slide head.

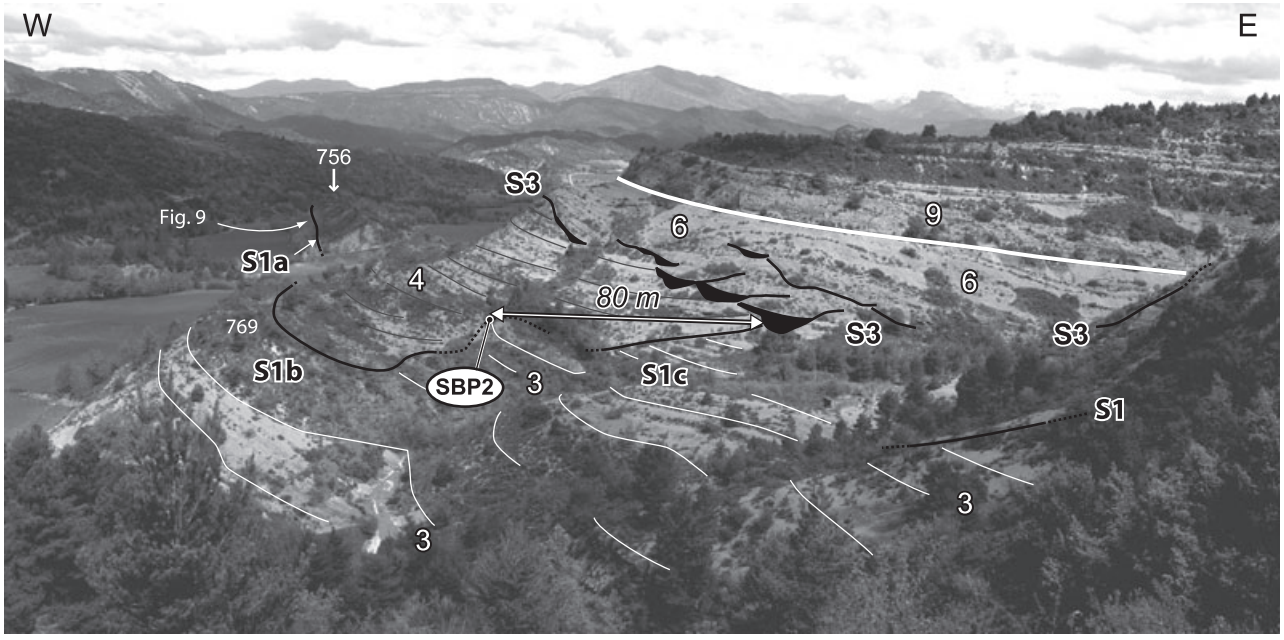

Fig. 11. The S1a to S1c composite slide surface and the S3 erosive surface on right bank of the Barranco el Solano. SBP is the slope breaking point of the S1 surface. '3' *in situ* layers of the Las Gorgas Composite Sequence (LGCS); '4' sedimentary infilling of the S1a and S1b scars; '6' the S3 sandy infilling with laminated sandstone lenses (in black) over five minor erosive surfaces that developed successively upward and westward (=Biñas d'Ena sequence deposits); '9' deposits of the Barranco el Solano Composite Sequence above the boundary of the LGCS (white heavy line).

Both parts are cut by an elementary slide surface covered by lenticular sandy layers of resedimented Nummulites. The onlap of the layers to the north-east corresponds to a right bank deposit, while flute casts and the imbrication of the Nummulites show a current toward the north-west. Such resedimentation of the Nummulites suggests a low sea-level deposit.

S1b, the middle segment of surface S1, again corresponds to a right bank (Fig. 11). A sliding direction toward the north-west is indicated by the extensive syn-sedimentary deformation of a step-shaped sandstone bed, fault strikes are from 40°N to 85°N. To the south-east, the shallowest S1c segment of surface S1 is still a right bank (Fig. 11). The infill is composed of a basal lag deposit of Nummulites covered with mudstone beds.

Surface S2 can be observed over a length of 400 m between Barranco Fuente Mazana (Wadsworth, 1994) and Biñas d'Ena (Fig. 4). This S2 surface cuts the sedimentary infilling or the cover of the S1 surface that represents its own relative substratum. Only the base of the left bank of the basal slide surface is exposed with an angular unconformity of about 15° between *in situ* layers

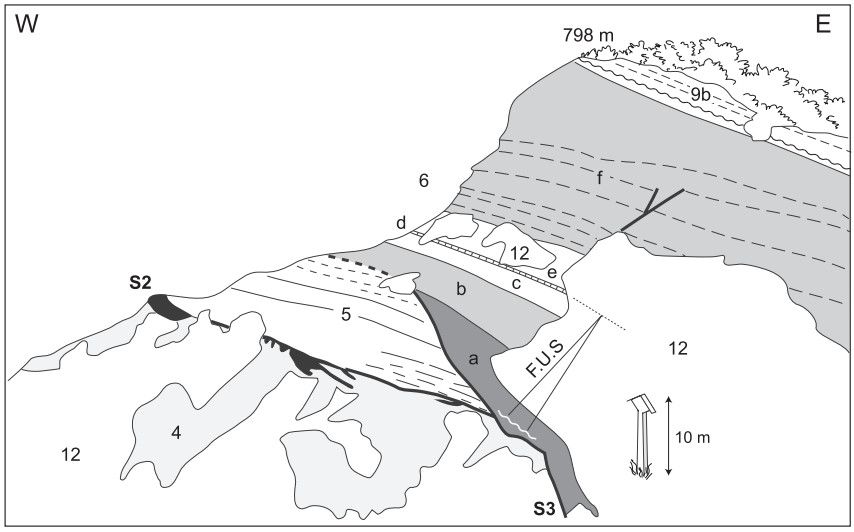

Fig. 12. Picture of the S2 and the S3 slide surfaces on the right bank of the Barranco Mazana. The S2 surface is marked by sandstone bodies: deformed horizontal wedges, small vertical dykes and step-shaped displaced beds. The S3 surface cuts about 10 m above the infills of S2 '5' and S1 '4', and disappears to the west where *in situ* layers and cover are conformable. '4' Sedimentary infilling or cover of the S1 scar. '5' Sedimentary infilling or cover of the S2 scar. '6' Sedimentary infilling and cover of the S3 surface successively composed of: 'a' sandstones and siltstones; 'b' lower siltstones; 'c' lower marlstones; 'd' limestone bed (F-US) fining-upward sequence 'a' to 'd'; 'e' upper marlstones; 'f' upper siltstones and sandstones (=Biñas d'Ena sequence deposits). '9b' Fossil-rich transgressive base of the Barranco el Solano Composite Sequence.

and the infilling. The sliding direction was towards the north-west, indicated by the orientation of clastic vertical dykes (striking from 7°N to 60°N) and extensive syn-sedimentary deformation of step-shaped sandstones with faults striking from 33°N to 100°N (Fig. 8). This surface could be related to a sliding surface observed 300 m to the north, west of Barranco as Peras (Fig. 4). The infill is preserved under the S3 surface and its cover, it is composed of 7 to 8 m of marlstones covered by 10 m of silty mudstones (Fig. 12).

Surface S3 can be observed on both sides of Barranco el Solano (Figs 4, 11 and 12) from its head scarp 250 m south of Barranco el Solano (Dreyer *et al.*, 1999) to its left bank north of Barranco Mazana (Wadsworth, 1994). This S3 surface corresponds to a 15 m deep and more than 400 m wide scar with a general orientation facing the north. It cuts the siltstone deposits of the LGCS and the sedimentary infillings and covers of the S1 and S2 surfaces (Fig. 12). No soft-sediment deformation was observed along this surface.

High values (up to 45°) of angular unconformity between *in situ* sandy layers and infilling layers can be observed at the head of the scar. The base of the upslope scarp is covered by 4 m of resedimented deposits: (i) lens-shaped bodies composed of tilted thin-bedded sandstone and mudstone layers; and (ii) a thick structureless sandstone bed with numerous clay chips.

Other high values of angular unconformity are observed northward along the left bank but resedimented deposits are not observed elsewhere along this S3 surface. On the left bank of the Barranco Mazana, the S3 infilling consists of about 10 m of cross-laminated sandstones overlain by horizontally laminated siltstones ('a', Fig. 12). Infilling deposits overlap the surface and the cover lies conformably on the top of S2 infilling ('b', Fig. 12). The lower part of this cover is 16 m thick and is composed of a fining-upward sequence (laminated siltstones, laminated silty marls and a 50 cm thick limestone bed: 'b', 'c' and 'd', respectively, Fig. 12).

Southward, on the right bank of Barranco el Solano (Fig. 11), the S3 surface is composed of five erosional surfaces that develop successively upward and westward. The sandy infilling of each surface starts with hummocky cross-stratified sandstones. This S3 surface may have been formed by the erosion resulting from a relative sea-level drop, when its infill and cover sedimentation has occurred during the following lowstand and highstand; they both constitute the new described Biñas d'Ena sequence.

Surface S4 can be observed from Biñas d'Ena to the north of Barranco Espuña (Fig. 4). The southern segment S4a lies on both sides of Barranco as

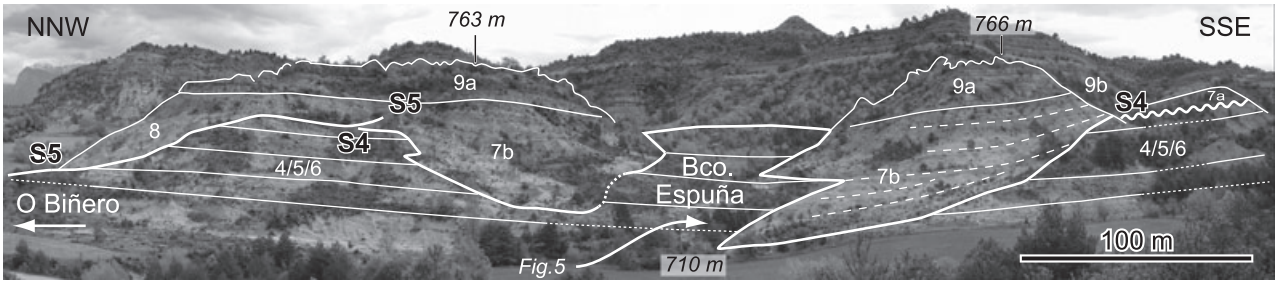

Fig. 13. Panoramic view of the S4 and S5 slide surfaces on both sides of Barranco Espuña. The S4 Barranco Espuña surface deeply cuts *in situ* layers, up to 130 m in the top of the LGCS (S1, S2 infilling and Biñas d'Ena sequence). The scar has been filled progressively by tilted blocks, slumped beds and some debris flow separated by *in situ* deposits. '4' and '5' Infilling resting above the S1 and S2 surfaces; '6' deposits of Biñas d'Ena sequence; '7a' Barranco as Peras sandstone body; '7b' Barranco Espuña resedimented and *in situ* deposits; '9' Barranco el Solano Composite Sequence deposits; '9a' upper infilling of the S4 and S5 scars; '9b' marlstones and Buil Nummulite banks. The angular unconformity between *in situ* and filling layers is from 23° to 34°. On the left, only the upper part of the head scarp and of the infill '8' of the S5 O Binero surface can be observed.

Peras where it incises up to 30 m of the marly top of the Biñas d'Ena sequence along 350 m. This segment is covered by the Barranco as Peras sandstone body. As for the S3 surface, the erosive surface and the sandstone body may result from a relative sea-level drop and its consecutive low-stand. The northern segments S4b, S4c and S4d are exposed on both the sides of Barranco Espuña (Fig. 13); they correspond to the right bank of the sliding surface. South of the Barranco the S4 surface appears as the head scarp of a composite slide surface where the angular unconformity between *in situ* and infilling layers is from 23° to 34° (Fig. 5). The substratum is deeply incised, up to 130 m both in the base of BSCS and at the top of LGCS (S1, S2 and S3 infilling). The sliding direction can be interpreted as being toward the north-west from the relative positions of its right bank and head scarp. The lower part of the scar has been filled by alternating tilted mudstone beds, cohesive debris flow and *in situ* mudstones and marlstone deposits (7b, Figs 4 and 5). Most of the upper part of the infilling is composed by likely *in situ* deposits with an upward progressive increase in the dip values. The highest layers of the infilling (9a, Figs 4 and 5) exhibit the same dip values as the truncated layers of the substratum. This observation is an indication that both the substratum and the infilling of S4 have been tilted by the growth of Boltaña anticline after the complete infilling had occurred. The cover of the infill is made of the marly layers of the high sea-level of the BSCS (9b, Fig. 4). Minor slumps are observed elsewhere both in the upper part of the infill and in the marly cover.

Surface S5 can be observed on both sides of the road to Arcusa, from Barranco Espuña to the north of O Binero crest where it cuts the down-slope part of S1 and S2, the cover of S3, a part of S4 infilling (Figs 4 and 13), the Las Gorgas sandstones and the marly beds of the top of the CCS (Dreyer *et al.*, 1999). The substratum is incised deeply, up to 160 m, and an angular unconformity reduces from 40° in the south to 0° in the north where the S5 surface disappears under Quaternary deposits (Fig. 4). When back-tilted from dip values of the *in situ* layers, the slide surface appears to face a north-west to north direction (strike measurements of the slide surface are from 58°N to 80°N). The lower part of the scar has been filled by tilted beds and *in situ* mudstones and marlstones. The upper part and the cover of the infilling join the corresponding deposits of surface S4 (9b, Fig. 4).

Surface S6 is located north of Fuente Espuña along the road to Santa Maria de Buil (Fig. 4). The incision cuts the top of the *in situ* layers up to 25 m in both the Buil Nummulite banks and the top of the underlying marly layers of the BSCS (De Federico, 1981) that are separated by a very low angular unconformity observed south of Fuente Espuña. The scarp dip reaches values up to 35° and gradually decreases to zero both upslope and downslope (Fig. 6). The base of the infilling is composed of a large horizontal sandy raft (up to 9 m thick and 130 m long). In the north (10a, Fig. 6) the raft is made up of horizontal fine sandstone layers that are deformed poorly and segmented by few vertical sandy dykes. In the south the raft thickness reduces, the layering is completely lost and deformation is more important and heterogeneous: the sandstone layer is cut by some vertical sandy dykes or is brecciated partially (10b, Fig. 6). At the southern termination

of the raft, the scarp base deposits consist of a complex wedge of laminated sandstones and mudstone-slumped layers covered with mud-supported sandstone clasts (10c, Fig. 6). The southern part of the raft and the slump and breccia deposits are covered by a succession of four horizontal wedges of coarse to medium-grained laminated sandstones. The wedges are about 15 m long and 1·5 to 2·9 m thick (10d, Fig. 6). The infilling continues with the last Buil Nummulite banks that overlap the slide surface (10e, Fig. 6). The remaining depression (10f and 10g, Fig. 6) has been filled completely by about 20 m of laminated marlstones and 2·5 m of structureless marlstones with many small ferruginous nodules (oxidized pyrite). The dip of the slide surface S6 faces towards the west and the overall north to south organization of the sandy raft and of the sandy wedges suggest that this outcrop exposes the right bank of a slide that had relocated toward the west to north-west direction.

To the north, the upper part of the deposits of the Barranco el Solano Composite Sequence is cut by another surface that probably corresponds to the head of the Barranco Rotal slump scar (Dreyer *et al.*, 1999). As this scar is located mainly out of the study area, it has not been investigated but it is distinguished from the S6 surface in the geological map (S6′, Fig. 4). Both the infilling of the Fuente Espuña and of the Barranco Rotal surfaces were truncated by an upper undifferentiated surface and covered by laminated limestone beds of the last marine levels from the Barranco el Solano Composite Sequence and then by the fluvial deposits of the Buil Composite Sequence (BCS).

Five out of the six surfaces documented in this paper from the Sobrarbe deltaic complex have been identified on the basis of the angular unconformity between the substratum and the filling layers in the head of the slide (Area 1 in Fig. 7). The directions and dips of the slide surfaces and the angular unconformity between the *in situ* layers and the sedimentary infilling have been measured all along the outcrops. A synthetic shape of the slides can be deduced from these measurements (Fig. 14). All the data have been corrected from the dip value of the substratum because most of the tilting of the layers was produced by the growth of the Boltaña anticline after the sediments were deposited. The general shape of the restored data shows that most of the slide surfaces trend about 55° N (facing north-west), with dip values from 20° to 40° toward the north-west. The extreme values indicate 150° N directions with dips to the south-west and 140° N with dips to the north-east; they may represent the lateral banks of the slides with dip values up to 30° (Fig. 10A).

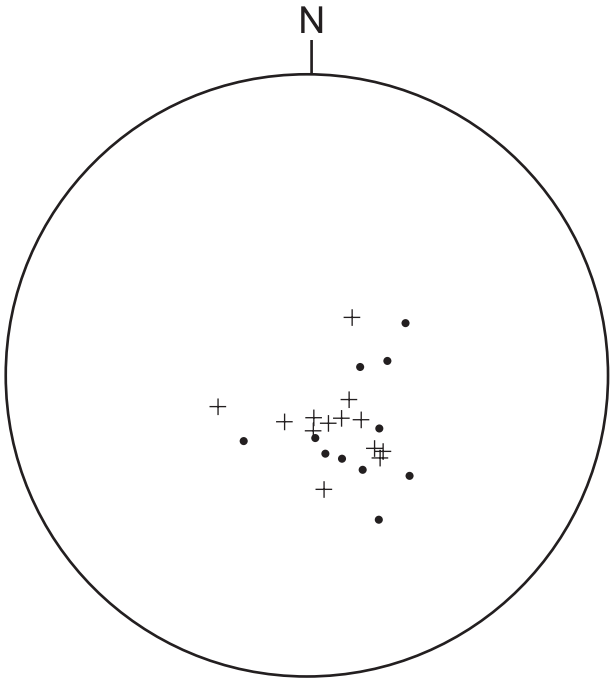

Fig. 14. Measurements of pole of the scarp plane as dots and the pole of the first layer of infilling planes as crosses (Wulff stereonet, lower hemisphere). All the data have been corrected from the dip value of the substratum. Most of the data are oriented about 55° N, with dip values from 20° to 40°, i.e. most of the slides face a north-west direction. The extreme values indicate 150° N directions with dips to the south-west and 140° N with dips to the north-east; they represent lateral banks of the slides with dip values up to 30°.

Three-dimensional modelling

The principal aim of this research was to build a 3D geological model in order to better describe the geometry of the slide surfaces through various graphical representations. To improve the field mapping of the surfaces (Fig. 4) and to reconstruct their 3D geometry, accurate topographic data provided the position of each slide surface in three dimensions.

High-precision topographic data were measured with a total station LEICA TCR 110 (Leica Geosystems, St Gallen, Switzerland). The precision of this measuring device is ±5 mm over a distance of 500 m and the vertical precision is within a few centimetres. Two operators are needed to take the measurements. The first one deals with the total station and guides the second operator to the location of the surface being measured. The second operator is on the surface

with the reflecting target of the apparatus. Both operators control the accurate position of the surface, one on the outcrop and the other at some distance. The operators communicate by radio throughout the process. The coordinates of 280 points belonging to the six sliding surfaces have been measured in this way within the study area. This methodology results in the building of a 3D architecture of the outcrops, including their geometry, and permits the analysis of the topographic data.

A 3D geological database is the representation of geological units and structures seen as actual volumes following a 3D matrix (x, y, z) at a given time (t) (Dhont *et al.*, 2005). Such a database is constructed from surface information only: the topography and the outcropping boundaries between the geological units.

The topography is represented numerically from a digital elevation model (DEM) generated by interpolation at 1·25 m ground pixel of 10 m interval contours from a digitized topographic map at the scale 1:25 000. Both the field mapping of the sliding surfaces and the DEM have been georeferenced in UTM coordinates and combined.

Each slide surface, identified in the field, corresponds to a mapped geological contour line represented by a collection of points defined by four variables: the spatial coordinates (x, y and z) and the time (t) corresponding to an isochronous line defining the age of the slide. The composite sequence boundaries and the sedimentary bodies have been drawn onto the DEM from geological mapping complemented by aerial orthophotos.

A 3D modeller (Earth Vision®; Dynamic Graphics, Inc., Alameda, CA, USA) was used to generate the surfaces (two-dimensional grid) passing through the points of each slide surface. The 2D grids were modified until their intersection with the DEM fitted the mapped contour lines. Each time the input data set was modified, the entire 3D geological model was recalculated in a trial and error process, i.e. by iteration towards an acceptable solution. Present-day submarine slides (Canals *et al.*, 2004; Haflidason *et al.*, 2004; Silva *et al.*, 2004) have provided 3D reference shapes that have been used to build the 3D geometry of the slump scars inside the model, where they are not observed. The validation of the resulting 3D model is obtained when there is a close to perfect match between the mapping of the slide surface contours and the intersections of the calculated slide surfaces with the DEM.

The volume of each layer is limited by the slide surfaces and the model boundaries (top, bottom and DEM). Each volume is displayed by one homogeneous colour that may represent either the part of the sedimentary infilling preserved over the basal slide surface or the deposit of each regional composite sequence as defined by Dreyer *et al.* (1999). One key sedimentary body was distinguished and referred to as the Las Gorgas sandstones.

The 3D model results from the superimposed succession of 11 coloured volumes (Fig. 15). In stratigraphic order, these volumes correspond to: (1) the last deposit of the CCS; (2) the Las Gorgas sandstone body corresponding to the base of the LGCS; (3) the marly distal part of the LGCS; (4) and (5) the deposits resting above the two oldest successive slide surfaces that truncate the LGCS (S1 and S2 surfaces); (6) the deposits of Biñas d'Ena sequence above the S3 erosional surface; (7) the infilling of the S4 erosional and slide surfaces; (8) the infilling of the S5 slide surface; (9) the undifferentiated deposits of the Barranco el Solano Composite Sequence (BSCS); (10) the infilling of the S6 and S6′ slide surfaces; and (11) the last marine levels of the BSCS and the base of the BCS.

The end-user of the model can examine the 3D model from various aspects (Fig. 15A), can slice it to generate cross-sections (Fig. 15B) or can disassemble it to examine individual slide surface units. The 3D geometric model provides estimates of the volume of each sedimentary body within the limits of the observed area. From such data, it is then possible to compare the ratio of slide-infilling sediments to bulk *in situ* deposits. For LGCS the part of the three successive infillings of S1, S2 and S3 represents 32×10^6 m^3, i.e. 12% of the entire deposit volume of the composite sequence. For the BSCS, the corresponding part of S4, S5 and S6 is $15{\cdot}4 \times 10^6$ m^3 and represents 13% of the volume of the composite sequence. These values for displaced volumes are within 10% to 15% of the deposit volume; they are equivalent to the estimation proposed by Dreyer *et al.* (1999). The part of the displaced volumes is of the same amount as those observed in present-day slides (see, for example, McAdoo *et al.*, 2000; Mienert *et al.*, 2002; Canals *et al.*, 2004; Hühnerbach & Masson, 2004).

INTERPRETATION AND DISCUSSION

The observation of the successive scar surfaces of the Sobrarbe deltaic complex has permitted the

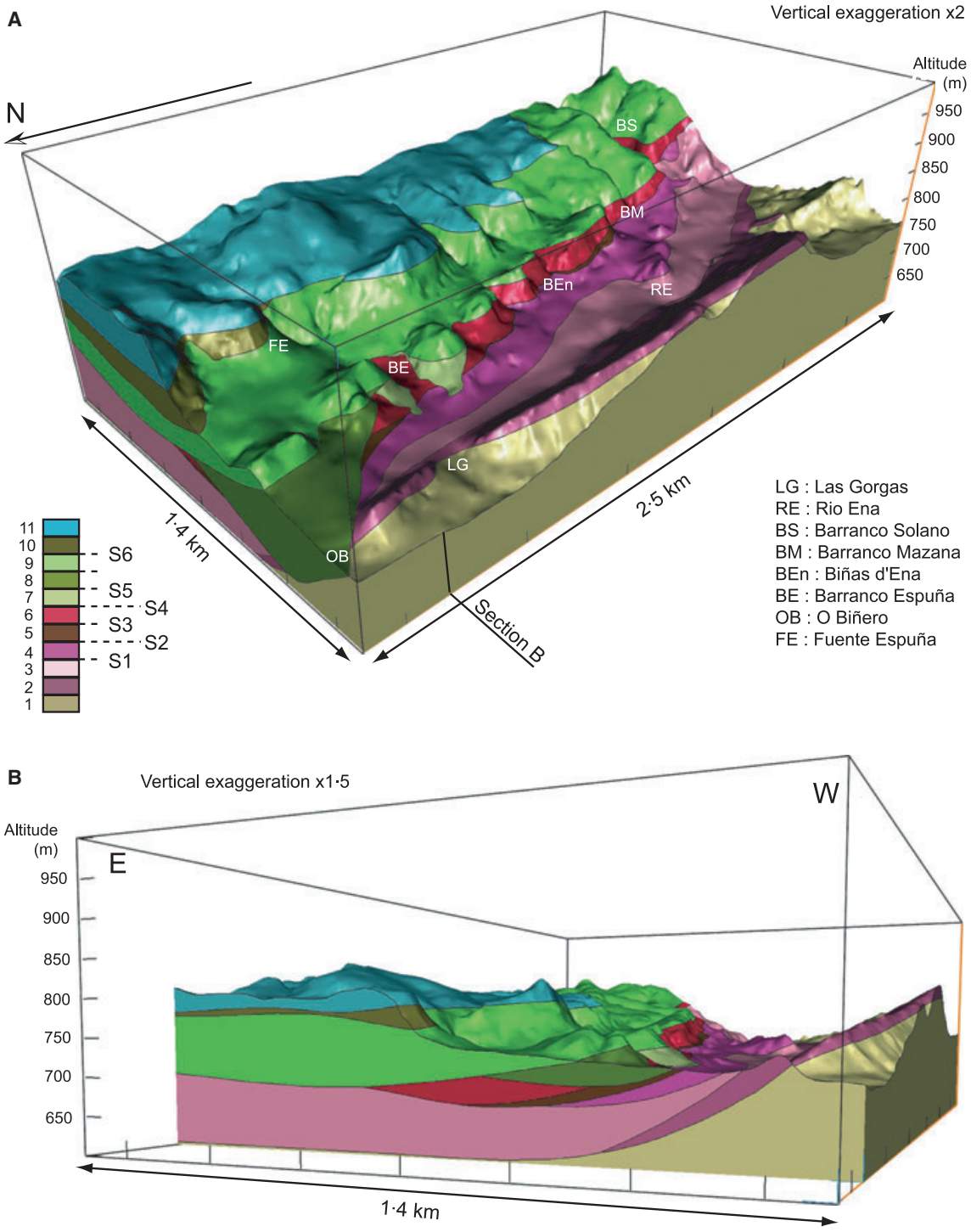

Fig. 15. Three-dimensional model constructed with the 3D modeller Earth Vision®. (A) View of the 3D model with the six slide surfaces and the localization of the places cited in the text. Quaternary deposits have not been included in the model. (B) East–west vertical section, slides piled up and cut the older infills. In stratigraphic order, numbers correspond to: (1) the last deposit of the Comaron Composite Sequence (CCS); (2) the Las Gorgas sandstone body corresponding to the base of the Las Gorgas Composite Sequence (LGCS); (3) the marly distal part of the LGCS; (4), (5) and (6) the deposits resting above the three first successive slide surfaces that truncate the LGCS (the S1, S2 and S3 surfaces); (7) the first infilling of the S4 slide surface; (8) the first infilling of the S5 slide surface; (9) the deposits of the Barranco el Solano Composite Sequence (BSCS); (10) the infilling of the S6 slide surface; (11) the last marine levels of the BSCS and the base of the Buil Composite Sequence (BCS).

characteristics of soft-sediment deformation along the slide surfaces to be shown and has provided information on the sedimentation rate inside a simple slump scar. The progressive development and infill of a composite scar surface has been shown, as well as the successive development of the different slide surfaces of a collapse complex structure. As a result, a conceptual model of the different stages of the slide scar development and infill can be proposed. Finally, the possible triggering mechanisms responsible for the Lutetian Sobrarbe instabilities have been identified, using some local data.

Soft-sediment deformation along the slide surface

No mineralization or calcite fibres were observed along the rupture surfaces that cut the substratum beds, indicating that the *in situ* layers were not lithified completely at the time of the slide event. Nevertheless, other observations suggest that sediments of the *in situ* layers were already sufficiently cohesive to have preserved the marks of bioturbation, such as burrows, of erosion structures, such as flute casts, and of mode I rupture, such as vertical cracks.

Both the fine-grained sandstones *in situ* layers and the Nummulite-rich resedimented marls of the filling sediments have been mixed together by bioturbation processes across the S6 surface (Fig. 16). At the time of failure, the burial depth of the fine-grained sandstones of the substratum was about 20 m. Some flute casts were observed on the S1, S2, S4 and S6 surfaces where the marlstones have been eroded. The vertical cracks that have been filled with coarse-grained sand were opened in the muddy layers of the substratum of the S1 and S2 surfaces. Along the S1 surface the burial depth, at the time of sliding, had reached about 170 m. The mode I opening of these extensional cracks requires some cohesion of the sediments in which they form (Price, 1966; Engelder, 1987; Price & Cosgrove, 1990). Because no mineralization has been observed along the rupture surfaces and because the sand has not been dissociated completely, these sandstone layers have been deformed when sediments were soft and moderately cohesive but not completely lithified.

The same grade of consolidation, at the time of sliding, is observed in displaced sediments. Some sandstones of the *in situ* layers were resedimented as rafts embedded in mudstones and translated without tilting; they may be soft deformed by small-scale normal faults (Fig. 8). Sandstone and mudstone layers have been resedimented with an increased degree of disorganization from large rafts to grain flow and debris flow layers.

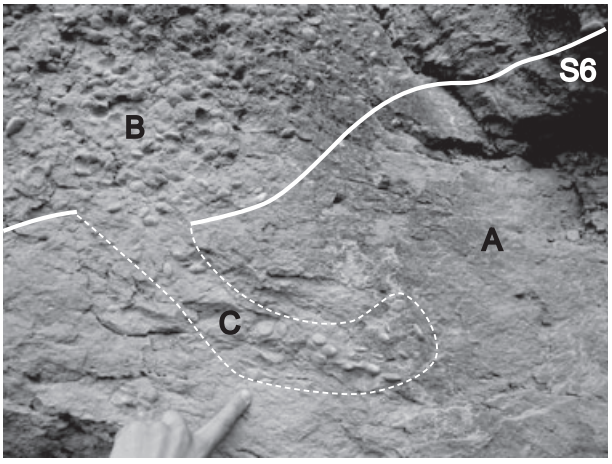

Fig. 16. At Fuente Espuña, the *in situ* layers and the infilling sediments have been mixed together by bioturbation processes across the S6 slide surface (outcrop located on Fig. 6); this is a clear indication that the lithification of the *in situ* layers was not achieved at the time where sliding occurred. 'A': Nummulite-free fine-grained sandstone (*in situ* layers). 'B': Nummulite-rich resedimented marls (infill sediments). 'C': Burrowed sediment across the S6 surface with Nummulites reworked downwards by bioturbation. The hand for scale is ~9 cm wide.

Sedimentation rate inside a simple slump scar

Deltaic sedimentation is composed of the succession of many events but, when considered over a long period of time, it can be seen as an almost continuous process. In the Sobrarbe prodelta, after the mass slide occurred, sedimentation continued and the first layers deposited in the scar successively draped the blocks that rest on the scar surface; these draping layers have onlapped the truncated layers of the scarp and then have draped the scar and its uphill shoulder where no visible unconformity can be observed (Fig. 7). As observed, the thickness of the draping layers increases downslope, in the infilling of the depression (Fig. 7). The available space created by the slide was filled completely, while a few metres of continuous sedimentation accumulated on the uphill shoulders of the slides. The depression of Fuente Espuña slump scar (S6 elementary surface) provides an example of marlstone infilling, where about 20 m of sediments correspond to 2 m of *in situ* deposits on the uphill shoulder (Fig. 6), not corrected for compaction. The corre-

sponding sedimentation rate is then *ca* 10 times higher in the scar than on the uphill shoulder. Using the rate of 87·5 to 70 cm per 1000 years as a mean value for *in situ* sediments, and because the scar is filled when 2 m of the *in situ* sediments are deposited, the time required to completely fill the scar is about 2500 years.

Such high values of sediment accumulation rates in the slump scars can be supposed as being the rule in the Sobrarbe Deltaic complex during late Lutetian period. A fast sediment accumulation rate is one of the factors considered to lead to increased porosity and pore-fluid pressure and to trigger sedimentary instabilities (Mienert *et al.*, 2002; Sultan *et al.*, 2004).

Progressive development and infill of a composite scar surface

The Barranco Espuña major slide surface (S4) provides a good example of the relationships between a composite slide surface and the progressive infill of the scar (Figs 5 and 13). On the left bank of the Barranco Espuña, the S4 surface appears to be composed of three elementary surfaces separated by two slope breaking points (Fig. 5, S4a, S4b and S4c). To the south, the S4b and S4c elementary surfaces cannot be distinguished and the S4 surface appears to be more regular (Fig. 13). The major slide scar infill is composed of alternating sets of apparently *in situ* regularly bedded mudstone deposits and displaced sediments such as tilted beds or debris flows. Three elementary slide surfaces are recognized at the base of the displaced sediments. Both the lower and upper elementary surfaces branch on the S4b and S4c surfaces, while the intermediate surface is independent of S4. As a result, the S4 scar appears to be characterized by three phases of retrogressive sliding (a, b and c) and composed of at least four infilling phases of displaced to *in situ* sediments. The surface S1 (S1a, b and c) shows another example of the progressive development of a composite slide surface with the progressive infill of the scar but, unfortunately, it is largely covered by Quaternary deposits.

Successive development of the different surfaces of a collapse complex structure

The major fossil collapse complex of Barranco el Solano slump (Dreyer *et al.*, 1999) can be subdivided into two collapse complex structures, separated by the deposits of the newly described Biñas d'Ena elementary sequence and bounded by two regressive surfaces. The lower collapse complex, Barranco Mazana complex, includes the S1 and S2 surfaces. The basal S1 surface is a composite and retrogressive slide surface. The S2 surface cuts the infilling of the S1 scar surface. These oldest scars stack one above the other and the only noticeable shifting is observed in the progressive retrogression of S1a to S1c head scarps.

The Biñas d'Ena elementary sequence starts with the formation of the S3 incision surface due to a relative sea-level drop. It is composed of the fining-upward sequence already described above the S3 surface and the coarsening-upward sequence that followed (Fig. 12). Horizontally, grain-size progressively reduces from sandy Barranco el Solano deposits in the south to marly Biñas d'Ena deposits in the north. This sequence ends with the erosion of the southern segment of the S4 surface at Barranco as Peras (Fig. 4). The thickness of the Biñas d'Ena elementary sequence can be estimated at about 75 m.

The upper collapse complex, Barranco Espuña complex, includes the S4 and S5 surfaces. The head scarp of the S4 and S5 surfaces shift about 1·5 km to the north of the head scarp of the S1 and S2 surfaces. The S4 surface cuts most of the LGCS, down to 130 m deep. The S5 surface cuts the LGCS and the top of CCS more deeply, down to 160 m.

The northward shift of the upper collapse complex can be related to the relative sea-level drops recorded at the boundaries of the Biñas d'Ena elementary sequence. In each collapse complex, the slide surfaces appear to develop retrogressively and to stack successively. Sediment accumulation rates are inferred to be very high in the downward scars. Here, the sediments are compacted poorly and lithified and the porosity is high (Bartetzko & Kopf, 2007). This observation may be an important contributory factor to explain why minor instabilities preferentially occur in the infilling of composite scars.

At the scale of major slides, the time of recurrence is defined by the duration of the LGCS and BSCS to the number of slide surfaces. That is about 0·45 Ma to four slide surfaces and this corresponds to one major slide event every 112 500 years. When looking at elementary surface succession, four minor slides have occurred during the formation of both the S1 and S4 major slides. That is to say that the recurrence time for minor slides could be about four times shorter than for major slides, i.e. from 25 000 to 30 000 years.

Conceptual model for the development of the scars in the Sobrarbe delta

The slide surfaces at the front of the Sobrarbe delta have not been preserved equally. The largest surfaces are composites and have been progressively infilled. These surfaces are known from their upslope domains (S4 and S5 surfaces) or from the downslope domains (S1 and S2 surfaces) that are free of resedimented deposits resulting from the major slide event. The S6 surface is the only one to exhibit a scar in which the upslope part of such resedimented deposits has been preserved at the toe of the scarp. The analysis of the 3D geometry and of the progressive infill has led to the proposal of a conceptual model for the development of the scars of the Sobrarbe delta (Fig. 17).

Stage 1 is a regressive event that may have developed before the sliding. The occurrence of the S6 sliding event at the top of a regressive sequence has been noticed by Dreyer *et al.* (1999). This stage 1 has been observed along the southern erosive segment of the S4 surface where the upper layers of the *in situ* deposits have been incised and covered by the As Peras sandstone body before the major slide event occurred. Both incision and sandstone deposits have resulted from a relative sea-level drop before the S4 sliding event.

Stage 2 is the major sliding event. The upslope part corresponds to the scarp that is well-exposed along the S4 surface south of Barranco Espuña (Fig. 13), S5 (Fig. 13) and S6 (Fig. 6). The slope of these scarps may reach up to 40° (Fig. 14). Slope gradients progressively reduce and disappear to the downslope parts where they are replaced by a flat bottom that has been deformed by small-scale half grabens, normal faults and opened cracks observed along the S1 (Fig. 9) and S2 surfaces.

Resedimented deposits are observed along the S6 surface; they consist of poorly deformed rafts, the upslope part of which is completely disorganized, showing a wavy roof similar in appearence to the half grabens of the S1 surface. The rafts rest on the lower part of the scar, at the toe of the 25 m deep scarp, while the upper part of the scarp is free of resedimented deposits (Fig. 6). Above the S5 surface, that cuts up to 150 m, the displaced masses may correspond to the resedimented deposits that are observed 2000 m far to the north; they consist of a 15 m thick mass of disorganized mudstone and sandstone blocks and olistoliths floating in a marly matrix. Displacement of the removed sediments appears to be proportional to the depth of the scar and, of course, to the amount of the displaced volume.

A seismite has been observed in the Biñas d'Ena sequence only. There, between Barranco as Peras and Biñas d'Ena, some 3 or 4 m of silty mudstone layers have been hydroplastically deformed (Fig. 18). Below a sharp plane erosive upper surface, these layers exhibit large millimetre-size symmetrical pillows, probably resulting from an earthquake. Unfortunately, the younger slide surface S4 has removed the more distal sediments and the possible relationship with a corresponding slide surface can no longer be established.

Stage 3 starts immediately after the sliding and can be subdivided into three successive times: (i) the erosive formation of flute marks at the bottom of some half grabens; (ii) the deposition of coarse-grained sandstones with clay chips and fine plant fragments in the small half grabens and open cracks; and (iii) the deposition of horizontally laminated then structureless fine-grained sandstones and mudstones (Fig. 9). This succession records the catastrophic increase in hydrodynamism within the scar followed by its progressive decrease down to the normal low-energy conditions. This succession probably corresponds to a tsunamite deposit that has followed the sliding.

Stage 4 corresponds to the marly infilling of the scar after the major slide event in the normal conditions of the distal delta front. It is observed above the S1 and S6 surfaces (Fig. 6).

Stage 5 is observed only in large scars where retrogressive sliding has occurred. The normal sedimentation is disrupted by either minor inner slides or retrogressive slides; they increase the size of the initial scar as observed on surfaces S1b and S1c (Fig. 13) or S4b and S4c (Fig. 5). Each of the minor slides may be covered by tilted blocks or debris flows such as already described. Minor retrogressive slides have been observed up to three times in the S1 and S4 scars.

Stage 6 corresponds to the last infilling time of the scars. In the upslope part of the scar of the S4, S5 and S6 surfaces, the scarp surface is overlain by the onlapping strata of the infill until the unconformity has reduced and the last deposits are parallel to the *in situ* layers. Nevertheless, the last deposits may be displaced by thin slump sheets, as observed in the S4 and S5 upper part of the infill.

Stage 7 marks the evolution end time with the burial of the scar infill under the high sea-level marly cover. This effect is well-illustrated by the marls of the BSCS that overlie the S4 and S5 infill.

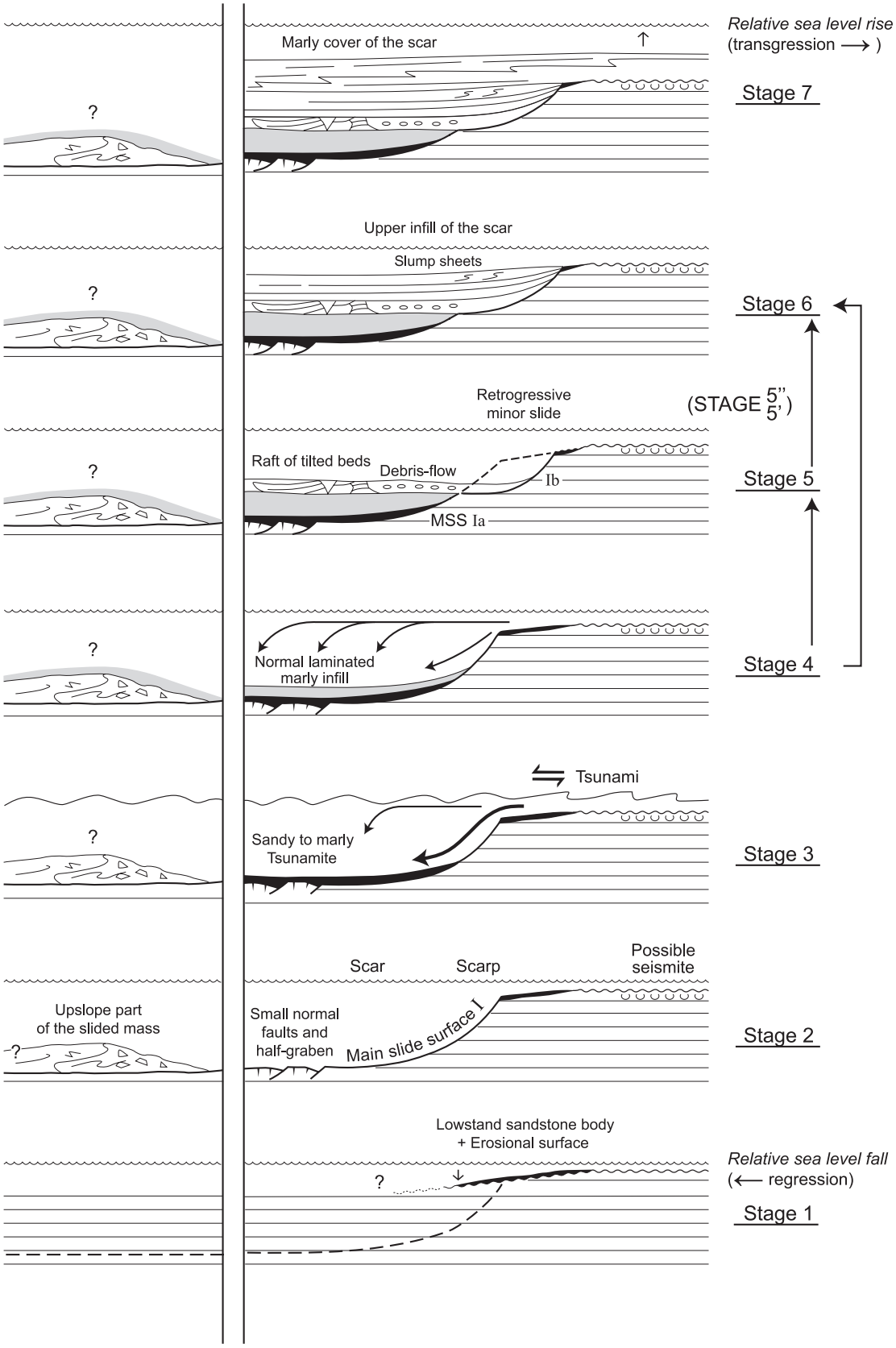

Fig. 17. Conceptual model of the development of the composite scars of the Sobrarbe delta, not to scale. The seven successive stages are described in the text.

Fig. 18. Large liquefaction pillows observed in silty mudstone layers of the Biñas d'Ena sequence. See location on Fig. 4. Open and black triangles, respectively, indicate the lower and upper erosive limits of the deformed level. These structures are interpreted as a seismite.

Triggering mechanisms for Sobrarbe instabilities

High values of sedimentation rate are known to favour formation of instabilities at a delta front (Nemec *et al.*, 1988; Moretti *et al.*, 2001). In such conditions, collapses result from both overloading due to sediment accumulation and high pore-fluid pressure due to under-compaction of fine-grained sediments (Postma, 1983; Gardner *et al.*, 1999; Bartetzko & Kopf, 2007). The sedimentation rate in the Sobrarbe delta ranges from 70 to 87·5 cm per 1000 years, a high value that makes the formation of slides easier. In the infill of the scars, where the sedimentation rate can be increased 10 times, the formation of superimposed slides is much easier. In no case has the instantaneous overload produced by events such as flood (Klein *et al.*, 1972) or storm waves (Nemec *et al.*, 1988) been observed in the Sobrarbe delta.

Relative sea-level fall has been proposed as a favourable condition for triggering instabilities (Mutti, 1985; Spence & Tucker, 1997; Dreyer *et al.*, 1999). A pronounced fall in relative sea-level has been associated with the slope instability of the S6 and S6′ surfaces that is observed at the top of BSCS (Dreyer *et al.*, 1999). Data from the present study show that an older relative sea-level drop has preceded the collapse of the Barranco Espuña complex along the S4 and S5 slide surfaces at the top of the Biñas d'Ena sequence. The marly deposits between these two collapse complexes seem to be coeval with the eustatic high sea-level of the so-called 'Biarritzian' transgression (Dreyer *et al.*, 1999). Conversely, the older relative sea-level fall associated with the S1 and S2 surfaces has been related to the tectonic uplift and tilting of the basin floor due to a growing phase of Arcusa anticline (Dreyer *et al.*, 1999). Both the seismite observed in the Biñas d'Ena sequence and the low angular unconformity that appears between the upper marly level and the lower Nummulite banks of BSCS south of Fuente Espuña, along an erosive surface, are other local proof of the regional syn-sedimentary tectonic activity. The largest part of the relative sea-level change could be related to the tectonic uplift, rather than to eustatic variations, according to the tectonic control on sedimentation of Ainsa Basin between the main South Pyrenean thrusts (Dreyer *et al.*, 1999; Pickering & Corregidor, 2005).

Apart from Biñas d'Ena, neither classical seismites structures nor sediment liquefaction have been observed in the studied prodelta area. The tectonic activity appears to be responsible for the relative sea-level changes but no direct relationship can be established between slides and possible seismic activity.

CONCLUSIONS

The field identification of five main successive fossil submarine slides in the western part of the Sobrarbe delta has made possible the characterization of associated sedimentary structures. In the upslope domain, most of the slide scarps trend about 55° N with dip values from 20° to 40° toward the north-west direction. The deduced sliding movement was toward the north-west direction. In the downslope domain, slide surfaces are identified by occasionally displaced deposits resting on the sole of the scar and, more generally, soft-sediment deformation structures. They are small normal faults that offset the scar surface and the *in situ* layers and that are associated with small extensive cracks (neptunian dykes) along the outer arc in small-scale rollover structures. It is proposed here that such small-scale associated structures can be used to recognize and trace the sliding surfaces where large displaced deposits are missing; they can also be helpful in assessing the sliding and its direction.

The restoration and mapping of the slides has led to a 3D model that provides an important data set showing the topography and the spatial organization of the five main slide surfaces and one erosional surface (S3). The S1, S2 and S3 surfaces developed mainly in the Las Gorgas Composite Sequence (LGCS), where they cut and are filled by LGCS sediments. The S4 and S5 surfaces developed in LGCS sediments but they are filled by sediments of the Barranco el Solano Composite Sequence (BSCS); they show the downward shifting of the unstable area from one sequence to the next, from the LGCS to the BSCS. The S6 surface developed in the BSCS. Each slide scar developed in a distal part of the Sobrarbe deltaic complex and cut a part of the infilling of the previous slide deposit. The 3D geometric model also provides estimates of the ratio of the slide infilling sediments to the bulk *in situ* deposits to be in the order of 12% to 13%. These values are similar to those observed in other work. The sedimentation rate inside a simple slump scar is estimated at 7 to 8·75 m/1000 years, that is about 10 times faster than the mean rate in the overall area of the Sobrarbe deltaic complex, and some 2500 years are required to fill a 25 m deep scar.

The successive development of the different surfaces of a collapse complex structure is illustrated by the major collapse complex of Barranco el Solano slump. It is subdivided into two collapse complex structures separated by the deposits of the newly described Biñas d'Ena elementary sequence bounded by two regressive surfaces. The northward shift of the upper collapse complex, 1·5 km away from the lower collapse complex, can be related to the relative sea-level drops recorded at the boundaries of the Biñas d'Ena elementary sequence. In each collapse complex, the slide surfaces appear to develop retrogressively and to stack successively. Here, the sediments are compacted poorly with high porosity which may explain why minor instabilities occur preferentially in the infilling of composite scars.

Finally, a conceptual model permits description of the development of the scars of the Sobrarbe delta from seven stages, starting with a regressive event and followed by: (i) the major slide event possibly associated with a seismite; (ii) deposition of a tsunamite; (iii) normal marly infilling; (iv) formation of one or more retrogressive minor slides; (v) filling-up of the scar; and (vi) burial of the scar under the high sea-level marly cover. The mechanisms responsible for triggering the Sobrarbe instabilities mainly correspond to three favourable related conditions that are: (i) high values of sedimentation rate; (ii) relative sea-level falls mainly controlled by tectonic uplift; and (iii) possible seismic activity.

ACKNOWLEDGEMENTS

This work benefited from the support of the 'instabilities' workgroup of the French CNRS-INSU GDR Marges project (2003–2006). We thank all the members of the Instabilities field workshop held in Ainsa (30 June and 1 July 2004) for constructive discussions. We thank Pascal Luxey for help in using the Earth Vision® 3D modeller and Christiane Cavaré-Hester for the line drawing of the figures. The revised version of the manuscript has benefited from the careful and constructive comments of P. Arbues, M. Moretti, K.T. Pickering and C. Puigdefabregas.

REFERENCES

Allen, J.R.L. (1982) *Sedimentary Structures: Their Character and Physical Basis*, Vol. II. Elsevier, Amsterdam, 663 pp.

Bartetzko, A. and **Kopf, A.J.** (2007) The relationship of undrained shear strength and porosity with depth in shallow (<50 m) marine sediments. *Sed. Geol.*, **196,** 235–249.

Callot, P., Sempere, T., Odonne, F. and **Robert, E.** (2008) Giant submarine collapse of a carbonate platform at the Turonian–

Coniacian transition: the Ayabacas Formation, southern Peru. *Basin Res.*, **20,** 333–357.

Canals, M., Lastras, G., Urgeles, R., Casamor, J.L., Mienert, J., Cattaneo, A., De Batist, M., Haflidason, H., Imbo, Y., Laberg, J.S., Locat, J., Long, D., Longva, O., Masson, D.G., Sultan, N., Trincardi, F. and **Bryn, P.** (2004) Slope failure dynamics and impacts from seafloor and shallow sub-seafloor geophysical data: case studies from the COSTA project. *Mar. Geol.*, **213,** 9–72.

Chapron, E., Beck, C., Pourchet, M. and **Deconinck, J.F.** (1999) 1822 earthquake-triggered homogeneite in Lake Le Bourget (NW Alps). *Terra Nova*, **11,** 86–92.

De Blasio, F.V., Elverhoi, A., Issler, D., Harbitz, C.B., Bryn, P. and **Lien, R.** (2004) Flow models of natural debris flows originating from overconsolidated clay materials. *Mar. Geol.*, **213,** 439–455.

De Federico, A. (1981) *La sedimentación de talud en el sector occidental de la cuenca Paleógena de Ainsa*. PhD thesis, Universidad Autónoma de Barcelona, Spain, 272 pp.

Dhont, D., Luxey, P. and **Chorowicz, J.** (2005) 3-D modelling of geologic maps from surface data. *AAPG Bull.*, **89,** 1465–1474.

Dreyer, T., Corregidor, J., Arbues, P. and **Puigdefabregas, C.** (1999) Architecture of the tectonically influenced Sobrarbe deltaic complex in the Ainsa Basin, northern Spain. *Sed. Geol.*, **127,** 127–169.

Engelder, T. (1987) Joints and shear fractures in rock. In: *Fracture Mechanics of Rock* (Ed. B.K. Atkinson), pp. 27–69. Academic Press Geology Series, New York.

Field, M.E., Gardner, V., Jennings, A.E. and **Edwards, B.D.** (1982) Earthquake-induced sediment failure on a 0.25° slope, Klamath River delta, California. *Geology*, **10,** 542–546.

Fisher, R.V. (1983) Flow transformations in sediment gravity flows. *Geology*, **11,** 273–274.

Frey Martínez, J., Cartwright, J. and **Hall, B.** (2005) 3D seismic interpretation of slump complexes: examples from the continental margin of Israel. *Basin Res.*, **17,** 83–108.

Frey Martínez, J., Cartwright, J. and **James, D.** (2006) Frontally confined versus frontally emergent submarines landslides: a 3D seismic characterisation. *Mar. Petrol. Geol.*, **23,** 585–604.

Gardner, J.V., Prior, D.B. and **Field, M.E.** (1999) Humboldt slide – a large shear-dominated retrogressive slope failure. *Mar. Geol.*, **154,** 323–338.

González, J., Schmitz, M., Audemaerd, F., Contreras, R., Mocquet, A., Delgado, J. and **De Santis, F.** (2004) Site effects of the 1997 Cariaco, Venezuela earthquake. *Eng. Geol.*, **72,** 143–177.

Gradstein, F.M., Ogg, J.G. and **Smith, A.G.** (2004) *A Geologic Time Scale 2004*. Cambridge University Press, Cambridge, 589 pp.

Greene, H., Gardner-Tagget, J., Ledbetter, M., Barminski, R., Chase, T., Hicks, K. and **Baxter, C.** (1991) Offshore and onshore liquefaction at Moss Landing spit, central California – results of the October 17, 1989 Loma Prieta eathquake. *Geology*, **19,** 945–949.

Haflidason, H., Sejrup, H.P., Nygård, A., Mienert, J., Bryn, P., Lien, R., Forsberg, C.F., Berg, K. and **Masson, D.** (2004) The Storegga Slide: architecture, geometry and slide development. *Mar. Geol.*, **213,** 201–234.

Hühnerbach, V. and **Masson, D.G.** (2004) Landslides in the North Atlantic and its adjacent seas: an analysis of their morphology, setting and behaviour. *Mar. Geol.*, **213,** 343–362.

Huvenne, V.A.I., Croker, P.F. and **Henriet, J.P.** (2002) A refreshing 3D view of an ancient collapse and slope failure. *Terra Nova*, **14,** 33–40.

Klein, G.V., Melo, U. and **Della Favera, J.C.** (1972) Subaqueous gravity processes on the front of cretaceous deltas, Recôncavo basin, Brazil. *Geol. Soc. Am. Bull.*, **83,** 1469–1492.

Lastras, G., Canals, M., Hughes-Clarke, J.E., Moreno, A., De Batist, M., Masson, D.G. and **Cochonat, P.** (2002) Seafloor imagery from the BIG'95 debris flow, western Mediterranean. *Geology*, **30,** 871–874.

Locat, J. and **Lee, H.J.** (2002) Submarine landslides: advances and challenges. *Can. Geotech. J.*, **39,** 193–212.

Loncke, L., Gaullier, V., Bellaiche, G. and **Mascle, J.** (2002) Recent depositional patterns of the Nile deep-sea fan from echo-character mapping. *AAPG Bull.*, **86,** 7, 1165–1186.

Lucente, C.C. and **Pini, G.A.** (2003) Anatomy and emplacement mechanism of a large submarine slide within a Miocene foredeep in the northern Apennines, Italy: a field perspective. *Am. J. Sci.*, **303,** 565–602.

Mandl, G. and **Crans, W.** (1981) Gravitational gliding in deltas. In: *Thrust and Nappe Tectonics* (Eds K.R. Mc Clay and N.J. Price), *Geol. Soc. London Spec. Publ.*, **9,** 41–54.

Martinsen, O.J. (1989) Styles of soft-sediment deformation on a Namurian (Carboniferous) delta slope, Western Irish Namurian Basin, Ireland. In: *Deltas: Sites and Traps for Fossil Fuels* (Eds M.K.G. Whateley and K.T. Pickering), *Geol. Soc. London Spec. Publ.*, **41,** 167–177.

McAdoo, B.G., Pratson, L.F. and **Orange, D.L.** (2000) Submarine landslide geomorphology, US continental slope. *Mar. Geol.*, **169,** 103–136.

Mello, U.T. and **Pratson, L.F.** (1999) Regional slope stability and slope-failure mechanics from the two-dimensional state of stress in an infinite slope. *Mar. Geol.*, **154,** 339–356.

Mienert, J., Berndt, C., Laberg, J.S. and **Vorren, T.O.** (2002) Slope instability of continental margins. In: *Ocean Margin Systems* (Eds G. Wefer, D. Billet, D. Hebbeln, B.B. Jørgensen, M. Schlüter and T. van Veering), pp. 179–193. Springer Verlag, Berlin.

Montenat, C., Barrier, P. and **Ott d'Estevou, P.** (1991) Some aspects of the recent tectonics in the Strait of Messina, Italy. *Tectonophysics*, **194,** 203–215.

Montenat, C., Barrier, P., Ott d'Estevou, P. and **Hibsch, C.** (2007) Seismites: an attempt at critical analysis and classification. *Sed. Geol.*, **196,** 5–30.

Moretti, M. and **Sabato, L.** (2007) Recognition of trigger mechanisms for soft-sediment deformation in the Pleistocene lacustrine deposits of the Sant'Arcangelo Basin (southern Italy): seismic shock vs. overloading. *Sed. Geol.*, **196,** 31–45.

Moretti, M., Soria, J.M., Alfaro, P. and **Walsh, N.** (2001) Asymmetrical soft-sediment deformation structures triggered by rapid sedimentation in turbiditic deposits (Late Miocene, Guadix Basin, southern Spain). *Facies*, **44,** 283–294.

Moscardelli, L. and **Wood, L.** (2008) New classification system for mass transport complexes in offshore Trinidad. *Basin Res.*, **20,** 73–98.

Mourgues, R. and **Cobbold, P.R.** (2003) Some tectonic consequences of fluid overpressures and seepage forces as demonstrated by sandbox modelling. *Tectonophysics*, **376,** 75–97.

Mulder, T. and **Alexander, J.** (2001) The physical character of subaqueous sedimentary density flows and their deposits. *Sedimentology*, **48,** 269–299.

Mulder, T. and **Cochonat, P.** (1996) Classification of offshore mass movements. *J. Sed. Res.*, **66,** 43–57.

Muñoz, J.A., McClay, K. and **Poblet, J.** (1994) Synchronous extension and contraction in frontal thrust sheet of the Spanish Pyrenees. *Geology*, **22,** 921–924.

Mutti, E. (1985) Turbidite systems and their relations to depositional sequences. In: *Provenance of Arenites* (Ed. G.G. Zuffa), pp. 65–93. NATO Advanced Scientific Institute, D. Reichel, Dordrecht, Holland.

Nemec, W., Steel, R.J., Gjelberg, J., Collinson, J.D., Prestholm, E. and **Oxnevad, I.E.** (1988) Anatomy of collapsed and re-established delta front in Lower Cretaceous of eastern Spitsbergen: gravitational sliding and sedimentation processes. *AAPG Bull.*, **72,** 454–476.

Nichols, R.J. (1995) The liquification and remobilization of sandy sediments. In: *Characterization of Deep Marine Clastic Systems* (Eds A.J. Hartley and D.J. Prosser), *Geol. Soc. London Spec. Publ.*, **94,** 63–76.

Papatheodorou, G. and **Ferentinos, G.** (1997) Submarine and coastal failure triggered by the 1995, Ms = 6.1 R Aegion earthquake, Gulf of Corinth, Greece. *Mar. Geol.*, **137,** 287–304.

Pickering, K.T. (1983) Small scale syn-sedimentary faults in the UpperJurassic ''Boulder Beds''. *Scot. J. Geol.*, **19,** 169–181.

Pickering, K.T. and **Corregidor, J.** (2005) Mass-transport complexes (MTCs) and tectonic control on basin-floor submarine fans, Middle Eocene, south Spanish Pyrenees. *J. Sed. Res.*, **75,** 761–783.

Piper, D.J.W., Cochonnat, P. and **Morrison, M.L.** (1999) The sequence of events around the epicentre of the 1929 Grand Banks earthquake: initiation of debris flows and turbidity current inferred from sidescan sonar. *Sedimentology*, **46,** 79–97.

Porebski, S.J. and **Steel, R.J.** (2003) Shelf-margin deltas: their stratigraphic significance and relation to deep-water sands. *Earth-Sci. Rev.*, **62,** 283–326.

Postma, G. (1983) Water escape structures in the context of a depositional model of a mass flow dominated conglomeratic fan-delta (Abrioja Formation, Pliocene, Almeria Basin, Spain). *Sedimentology*, **30,** 91–103.

Price, N.J. (1966) *Fault and Joint Development in Brittle and Semi-brittle Rock*. Pergamon Press, New York, 568 pp.

Price, N.J. and **Cosgrove, J.W.** (1990) *Analysis of Geological Structures*. Cambridge University Press, Cambridge, 502 pp.

Puigdefabregas, C., Muñoz, J.A. and **Verges, J.** (1991) Trusting and foreland basin evolution in the southern Pyrenees. In: *Thrust Tectonics* (Ed. K. McClay), pp. 247–254. Chapman & Hall, London.

Reading, H.G. (1996) *Sedimentary Environments: Processes, Facies and Stratigraphy*, 3rd edn. Blackwell Science, Oxford, 688 pp.

Remacha, E., Oms, O. and **Gual, G.** (2003) Sand-rich turbidite systems of the Hecho Group from slope to basin plain. Facies, stacking patterns, controlling factors and diagnostic features. Geological field Trip 12, South-Central Pyrenees. AAPG International Conference and Exhibition, Barcelona, Spain, September 21–24.

Serra-Kiel, J., Hottinger, L., Caus, E., Drobne, K., Ferrandez, C., Jauhri, A.K., Less, G., Pavlovec, R., Pignatti, J., Samso, J.M., Sirel, E., Strougo, A., Tambareau, Y., Tosquella, J. and **Zakrevskaya, E.** (1998) Larger foraminiferal biostratigraphy of the Tethyan Palaeocene and Eocene. *Bull. Soc. Géol. Fr.*, **169,** 2, 281–299.

Silva, A.J., Baxter, C.D.P., LaRosa, P.T. and **Bryant, W.R.** (2004) Investigation of mass wasting on the continental slope and rise. *Mar. Geol.*, **203,** 355–366.

Spence, G.H. and **Tucker, M.E.** (1997) Genesis of limestone megabreccias and their significance in carbonate sequence stratigraphic models: a review. *Sed. Geol.*, **112,** 163–193.

Spörli, K.B. and **Rowland, J.V.** (2007) Superposed deformation in turbidites and syn-sedimentary slides of the tectonically active Miocene Waitemata Basin, northern New Zealand. *Basin Res.*, **19,** 199–216.

Sultan, N., Cochonat, P., Canals, M., Cattaneo, A., Dennielou, B., Haflidason, H., Laberg, J.S., Long, D., Mienert, J., Trincardi, F., Urgeles, R., Vorren, T.O. and **Wilson, C.** (2004) Triggering mechanisms of slope instability processes and sediment failures on continental margins: a geotechnical approach. *Mar. Geol.*, **213,** 291–321.

Terzaghi, K. (1943) *Theoretical Soil Mechanics*. Wiley, New York, 510 pp.

Trincardi, F., Cattaneo, A., Correggiari, A. and **Ridente, D.** (2004) Evidence of soft sediment deformation, fluid escape, sediment failure and regional weak layers within the late Quaternary mud deposits of the Adriatic Sea. *Mar. Geol.*, **213,** 91–119.

Vendeville, B.C. and **Gaullier, V.** (2003) Role of pore-fluid pressure and slope angle in triggering submarine mass movements: natural examples and pilot experimental models. In: *Submarine Mass Movements and their Consequences* (Eds J. Locart and J. Mienert), pp. 137–144. Kluwer Academic Publishers, Dordrecht.

Vernhet, E., Heubeck, C., Zhu, M.-Y. and **Zhang, J.-M.** (2006) Large-scale slope instability at the southern margin of the Ediacaran Yangtze platform (Hunan province, central China). *Precambrian Res.*, **148,** 32–44.

Wadsworth, J.A. (1994) *Sedimentology and Sequence Stratigraphy in an Oversteepened Ramp Setting: Sobrarbe Formation, Ainsa Basin, Spanish Pyrenees*. PhD thesis, University of Liverpool, 195 pp.

Wilson, C.K., Long, D. and **Bulat, J.** (2004) The morphology, setting and processes of the Afen Slide. *Mar. Geol.*, **213,** 149–167.

Manuscript received 11 July 2007; revision accepted 2 October 2008